การสังเคราะห์เมมเบรนเพอรอฟสไกต์ความหนาแน่นสูงชนิด $La_{1-x}Sr_xGa_{1-y}Fe_yO_{3-\delta}$ ด้วยวิธีซิเทรตประยุกต์

นายสราวุธ ตันหยง

SYNTHESIS OF DENSE $La_{1-x}Sr_xGa_{1-y}Fe_yO_{3-\delta}$ PEROVSKITE MEMBRANE BY MODIFIED CITRATE METHOD

Mr. Sarawut Tanyong

Thesis Title   Synthesis of dense $La_{1-x}Sr_xGa_{1-y}Fe_yO_{3-\delta}$ perovskite membrane by modified citrate method

By   Mr. Sarawut Tanyong

Field of Study   Petrochemistry and Polymer Science

Thesis Advisor   Associate Professor Supawan Tantayanon, Ph.D.

Thesis Co-Advisor   Oravan Sanguanruang, Ph.D.

_____

        Accepted by the Faculty of Science, Chulalongkorn University in Partial Fulfillment of the Requirements for the Master 's Degree

        …………………………………Dean of the Faculty of Science
        (Associate Professor Wanchai Phothiphichitr, Ph.D.)

Thesis Committee

        ………………………………Chairman
        (Professor Pattarapan Prasassarakich, Ph.D.)

        ………………………………Thesis Advisor
        (Associate Professor Supawan Tantayanon, Ph.D.)

        ………………………………… Thesis Co-Advisor
        (Oravan Sanguanruang, Ph.D.)

        ………………………………Member
        (Associate Professor Wimonrat Trakarnpruk, Ph.D.)

        ………………………………Member
        (Nipaka Sukpirom, Ph.D.)

นายสราวุธ ตันหยง : การสังเคราะห์เมมเบรนเพอรอฟสไกต์ความหนาแน่นสูงชนิด La$_{1-x}$Sr$_x$Ga$_{1-y}$Fe$_y$O$_{3-\delta}$ ด้วยวิธีซิเทรตประยุกต์ (Synthesis of dense La$_{1-x}$Sr$_x$Ga$_{1-y}$Fe$_y$O$_{3-\delta}$ perovskite membrane by modified citrate method)
อาจารย์ที่ปรึกษา: รศ. ดร. ศุภวรรณ ตันตยานนท์ อาจารย์ที่ปรึกษาร่วม : อ. ดร. อรวรรณ สงวนเรือง, จำนวนหน้า 90 หน้า ISBN 974-17-3708-4

อนุภาคขนาดเล็กของแลนทานัมแกลเลตเพอรอฟสไกต์ออกไซด์ที่ถูกแทนที่ด้วยสตรอนเทียม และเหล็กชนิด La$_{1-x}$Sr$_x$Ga$_{1-y}$Fe$_y$O$_{3-\delta}$ เมื่อ สตรอนเทียม = 0.5 และเหล็ก = 0.8; สตรอนเทียม = 0.4 และเหล็ก = 0.6-0.8; สตรอนเทียม = 0.3 และเหล็ก = 0.3-0.8; และสตรอนเทียม = 0.2 และเหล็ก = 0.3-0.8 ซึ่งสังเคราะห์ด้วยวิธีซิเทรตประยุกต์และถูกเผาที่อุณหภูมิ 800$^{\mathrm{o}}$C และคัดเลือกผงเพอรอฟสไกต์ที่เป็นเฟสเดี่ยวหรือมีเฟสที่สองเพียงเล็กน้อยมานำขึ้นรูปเป็นเมมเบรนด้วยเครื่องอัดด้านเดียว (uniaxial pressing machine) จากนั้นนำไปซินเทอร์ที่อุณหภูมิ 1,200-1,350 $^{\mathrm{o}}$C เป็นเวลา 10 ชั่วโมง ทั้งผงและแผ่นเมมเบรนของเพอรอฟสไกต์จะถูกตรวจสอบลักษณะของเฟสเดี่ยวโดยเทคนิคการเลี้ยวเบนของรังสีเอกซ์ และตรวจสอบลักษณะพื้นผิวและภาคตัดขวางของเมมเบรนด้วยเทคนิคสแกนนิงอิเล็กโทรไมโครสโคปี พบว่า LSGF 6428 (เป็นสัญลักษณ์ที่มาจาก La$_{0.6}$Sr$_{0.4}$Ga$_{0.2}$Fe$_{0.8}$O$_{3-\delta}$), LSGF 6437, LSGF 7328, LSGF 7337, LSGF 7346, LSGF 8228, LSGF 8237 และ LSGF 8246 เป็นเฟสเดี่ยวหรือมีเฟสที่สองเพียงเล็กน้อย แต่ LSGF 5528, LSGF 7355, LSGF 7364, LSGF 8273, LSGF 8255, LSGF 8264 และ LSGF 8273 แสดงให้เห็นเฟสที่สองอย่างชัดเจน แสดงให้เห็นชัดเจนว่าเฟสที่สองจะเพิ่มมากขึ้นเมื่อปริมาณ Sr หรือ Ga เพิ่มขึ้น เพราะการแทนที่บางส่วนของ La และ Fe ด้วย Sr และ Ga ที่มีขนาดใหญ่กว่า สำหรับผลจาก XRD ของเมมเบรน พบว่าเฟสที่สองจะเพิ่มขึ้นตามอุณหภูมิซินเทอริง ดังนั้นจึงสรุปได้ว่าการเปลี่ยนแปลงเฟสของเพอรอฟสไกต์ชนิด La$_{1-x}$Sr$_x$Ga$_{1-y}$Fe$_y$O$_{3-\delta}$ ขึ้นกับอุณหภูมิซินเทอริง อธิบายได้จากการระเหยของ Ga ที่ที่อุณหภูมิสูง ทำให้เกิด LaSrGaO$_4$ หรือเฟสที่สองขึ้น

สาขาวิชา ปิโตรเคมีและวิทยาศาสตร์พอลิเมอร์   ลายมือชื่อนิสิต…………..…….................…...
ปีการศึกษา   2546   ลายมือชื่ออาจารย์ที่ปรึกษา………….…….……
ลายมือชื่ออาจารย์ที่ปรึกษาร่วม……………..….

4472439223   : MAJOR PETROCHEMISTRY AND POLYMER SCIENCE

KEY WORD: PEROVSKITE / OXYGEN SEPARATION MEMBRANE / LANTHANUM GALLATE

MR. SARAWUT TANYONG : SYNTHESIS OF DENSE $La_{1-x}Sr_xGa_{1-y}Fe_yO_{3-\delta}$ PEROVSKITE MEMBRANE BY MODIFIED CITRATE METHOD THESIS ADVISOR : ASSOC. PROF. SUPAWAN TANTAYANON, Ph. D. THESIS COADVISOR : ORAVAN SANGUANRUANG, Ph. D. 90 pp. ISBN 974-17-3708-4

The fine particle strontium and iron substituted lanthanum gallate perovskite oxides, $La_{1-x}Sr_xGa_{1-y}Fe_yO_{3-\delta}$ where Sr = 0.5, Fe = 0.8; Sr = 0.4, Fe = 0.6-0.8; Sr = 0.3, Fe = 0.3-0.8 and Sr = 0.2, Fe = 0.3-0.8 were synthesized by a modified citrate method and were calcined at 800°C. The single phase or some traces of secondary phase powder were selected for preparing the membrane discs using a uniaxial pressing machine. They were then sintered at $1,200\text{-}1350^{o}$C for 10 hours. Both types of powder and membrane were subjected to the single-phase determination by the X-ray diffraction. In addition, the surface and cross section of each membrane were investigated by scanning electron microscopy. It was found that LSGF 6428 (represented from $La_{0.6}Sr_{0.4}Ga_{0.2}Fe_{0.8}O_{3-\delta}$), LSGF 6437, LSGF 7328, LSGF 7337, LSGF 7346, LSGF 8228, LSGF 8237and LSGF 8246 showed the single phase or some traces of secondary phase but LSGF 5528, LSGF 7355, LSGF 7364, LSGF 7373, LSGF 8255, LSGF 8264 and LSGF 8273 showed the clearly observed secondary phase. It was obvious that the secondary phase increased when the amount of Sr or Ga increased because La and Fe were partially substituted by the larger ionic radii, Sr and Ga, respectively. For the XRD patterns of membranes, it was found that the secondary phase tended to form at increasing sintering temperature. Therefore, it indicated that the phase transformation of $La_{1-x}Sr_xGa_{1-y}Fe_yO_{3-\delta}$ perovskite depended on the increasing of sintering temperature. This can be explained by the vaporization of Ga at high temperature that caused the formation of $LaSrGaO_4$ or secondary phase.

Field of study Petrochemistry and Polymer Science   Student's signature   .

Academic year   2003   Advisor's signature   .

Co-advisor's signature   .

ACKNOWLEDGEMENTS

CONTENTS

CONTENTS (Continued)

CONTENTS (Continued)

CONTENTS (Continued)

LIST OF TABLES

LIST OF FIGURES

LIST OF FIGURES (continued)

LIST OF FIGURES (continued)

LIST OF SCHEMES

LIST OF ABBREVIATIONS

δ	Non-stoiciometry of oxygen in mole formula
MIEC	Mixed ionic-electronic conductor
r	Ionic radius
t	Tolerance factor
P'_{O_2}	Oxygen partial pressure at higher pressure
P''_{O_2}	Oxygen partial pressure at lower pressure
$V\ddot{o}_2$	Oxygen vacancies
h	Electron-holes
L	Membrane thickness
J_{O_2}	Oxygen permeation flux
SEM	Scanning electron microscopy
XRD	X-ray diffraction
BSCF	Perovskite containing Ba, Sr, Co, and Fe
BFM	Bubble flow meter
P	Pressure transducer
LSC	Perovskite containing La, Sr, and Co
LSGF	Perovskite containing La, Sr, Ga, and Fe

CHAPTER 1

INTRODUCTION

Recently, the attention of methane utilization has been considered due to the large amount of natural gas available to be upgraded for low-cost transportation fuels. Methane was used as a valuable raw material for several industrial processes, including the synthesis gas (syngas) production.

Syngas is a mixture of carbon monoxide and hydrogen, acts as a feedstock for the synthesis of ammonia and methanol. Additionally, it can be converted to higher hydrocarbons, alcohols and aldehydes [1]. Technologies available for converting methane to higher hydrocarbons or liquid fuels are classified as either direct or indirect routes. Direct conversion of methane requires direct partial oxidation to methanol, formaldehyde, or others, or oxidative coupling to ethylene. However, the direct conversion processes have not yet been successful because the desired products are more reactive than methane. Therefore, low product yield is normally encountered [2].

Nowadays, indirect conversion is the main process for producing syngas based on the steam reforming of methane as demonstrated in Equation 1.1, which is the main component of natural gas [3].

$$CH_4 + H_2O = CO + 3H_2 \qquad \Delta H_{800°C} \ +225 \ kJ/mol \qquad (1.1)$$

This is a highly endothermic reaction providing some disadvantages: high temperatures and pressures are required for methane conversions, and high temperature and high pressure resistant materials are needed. And a H_2/CO mole ratio is 3.0. This ratio is not the desired stoichiometry of some chemical reactions such as methanol and Fischer-Tropsch synthesis requiring H_2/CO mole ratios of 2.0. Another approach for syngas production originates from the energy demand of the steam reforming reaction, as this process requires energy input. The partial oxidation of methane to synthesis gas is a mildly exothermic reaction, Equation 1.2 that is free

from the above limitations of the steam reforming method. Moreover, the partial oxidation of methane has a H_2/CO mole ratio of 2.0 would be a viable alternative reaction to the methane steam reforming reaction for syngas generation [4]. However, the most significant cost associated with the partial oxidation is the oxygen supply.

$$CH_4 + 0.5O_2 = CO + 2H_2 \qquad \Delta H_{800°C} \;\; -23 \text{ kJ/mol} \qquad\qquad (1.2)$$

Dense ceramic membranes, particularly the mixed ionic and electronic conducting (MIEC) perovskite, represented by the general formula ABO_3, offer potential solutions to eliminate the need for constructing the oxygen separation plant. The technology substantially reduces the cost of converting natural gas to syngas by 30%, and could save the oil and gas industry millions of dollars annually. Several advantages of using the oxygen-ion conducting membrane reactor include achieving high product selectivity, employing air as the source of the oxidant while eliminating N_2 contamination in the product, circumventing flammability limits due to diffusion-limited operation, reducing a large part of the cost of gas compression in downstream processing, and avoiding the formation of environmental pollutant (NO_x) during high-temperature reactions [5].

The citrate method has been chosen in this study for the synthesis of lanthanum-based perovskites. The citrate method involves the complex of metal ions with citric acid and the spontaneous combustion. The advantages of the citrate method include less energy consumption and potential to get fine particles and a single phase powder [6].

1.1 The objectives of the thesis

    1.1.1   Synthesizing the single phase perovskite membranes.

    1.1.2   Synthesizing the dense perovskite membrane.

1.2 The scope of the thesis

1.2.1 Synthesis of fine particles of the single phase perovskites by using the modified citrate method.

1.2.2 Selecting the single phase perovskites to prepare membrane perovskite discs.

1.2.3 Study the effect of the sintering temperatures.

CHAPTER 2

THEORY

There are many perovskite compound types. They have various properties that are used in different applications such as insulators, dielectrics, magnetic materials, ionic conductors, mixed conductors, and superconductors. This study is focused on the use of mixed conducting perovskites as oxygen separation membranes for the methane partial oxidation reaction. This chapter includes the general review of structure and physical properties, synthesis methods, membrane preparation, the oxygen permeation through a perovskite membrane, and the reactor of oxygen permeation.

2.1 Structure of perovskites [7]

2.1.1 Crystal structure

The ideal perovskite-type structure is cubic with the unit formula of perovskite-type oxides ABO_3, A is a larger cation and B is a smaller cation. In this structure, the B cation is 6-fold coordinated and the A cation is 12-fold coordinated with the oxygen anions. Figure 2.1 depicts the corner sharing octahedral that form the skeleton of the structure, in which the center position is occupied by the A cation. Alternatively, this structure can be viewed with the B cation placed in the center of the octahedron and the A cation is in the center of the cube.

● **A ion**   ● **B ion**   ⬤ **O ion**
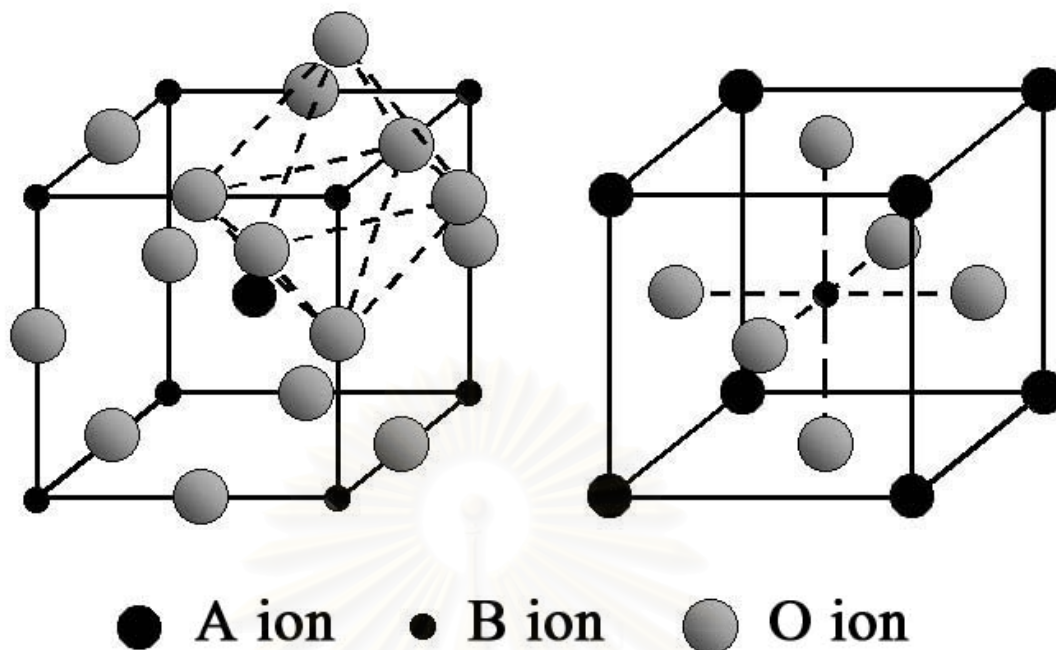
Figure 2.1. ABO$_3$ ideal perovskite structure showing oxygen octahedron containing the B ion linked through corners to form a three-dimensional cubic lattice.

In the ideal structure, where the atoms are touching one another, the B-O distance is equal to $a/2$ (a is the cubic unit cell parameter) while the A-O distance is $(a/\sqrt{2})$ and the following relationship between the ionic radius (r) holds: $r_A + r_O = \sqrt{2}(r_B + r_O)$. In general, the perovskite structure is formed if the tolerance factor, t, is in the range of 0.75-1.0

$$t = (r_A + r_O) / \sqrt{2}(r_B + r_O) \qquad (2.1)$$

The ideal perovskite is the cubic structure with the tolerance factor of 1.0. The perovskite structure is stable in the range 0.75< t <1.0, and is cubic in the range t > 0.95. [8, 9]

2.1.2 Nonstoichiometry in perovskites

The partial substitution of A and B ions giving rise to cation deficiency, anion deficiency, or anion excess affected to the formation of nonstoichiometry in perovskites. For the cation deficiency, A-Site cations can be absent without collapse of the perovskite structure because of the stability of the BO_3 group [8]. While B-site vacancies in perovskites are not stabilized because of the large formal charge and the small size of the B cations. However, an oxygen vacancy in perovskites is usual appeared more than a cation deficiency.

Oxygen-deficient in perovskites can be described in term of complex perovskite-related super-structures of general formula $A_nB_nO_{3n-1}$. The stacking manner structure depends on the size, electronic configurations, and coordination numbers of A and B cations. Oxygen vacancies were generated by the substitution of ions that similar size but different valence. For example, the La^{3+} ions in $LaBO_3$ are partially substituted with Sr^{2+} to form $La_{1-x}Sr_xBO_{3-\delta}$ perovskite. Therefore, the oxygen vacancies appeared.

2.2 Physical properties [7]

The ABO_3 perovskites display several interesting physical properties such as ferroelectricity ($BaTiO_3$), ferromagnetism ($SrRuO_3$), weak ferromagnetism ($LaFeO_3$), superconductivity ($YBa_2Cu_3O_7$), large thermal conductivity due to exciton transport ($LaCoO_3$), insulator-to-metallic transitions of interest for thermistor applications ($LaCoO_3$), a fluorescence compatible with laser action ($LaAlO_3$: Nd), and transport properties of interest for high temperature thermoelectric power (La_2CuO_4).

2.2.1 Magnetic properties

In the ideal cubic perovskite structure, each atom of oxygen is shared by two B^{3+} ions, forming a B-O-B angle of 180°. Such a configuration is favorable for super exchange interactions between magnetic B^{3+} cations. This exchange usually results in anti-parallel coupling of nearest-neighbor magnetic moments. When the B^{3+} ions are

in two sub lattices ($A_2BB'O_6$) the other spin arrangements are possible. If B' is a diamagnetic ion, the B^{3+} ions are aligned anti-ferromagnetic, and the most important exchange mechanism is believed to be a longer range super exchange interaction through two oxygen of the type B-O-B'-O-B. The B-B separation is now considerably longer than the 0.4 nm separation found in the ideal perovskite. The $LnFeO_3$ (Ln = lanthanide) perovskites are those that have attracted the most attention because of their possible applications as technological magnetic materials [9]. These compounds show a weak spontaneous magnetic moment, which is attributed to a slight canting of the iron moments, which are otherwise anti-ferromagnetic aligned. Similarly, $LnMnO_3$ shows very interesting magnetic properties. These manganites containing mostly Mn^{3+} or Mn^{4+} ions show anti-ferromagnetic behavior. However, ferromagnetic behavior is observed in the range from 25 to 35% Mn^{4+}. A weak magnetic interaction was found between Mn^{3+} ions, together with a negative interaction between Mn^{4+} ions and a strong positive interaction between Mn^{3+} and Mn^{4+}. A similar kind of behavior was found for the combination of Co^{3+} and Co^{4+}, but the Cr and Fe compounds were found to be anti-ferromagnetic.

2.2.2 Electrical properties

The electrical conductivity of perovskites also shows wide variations. Several compounds have been used for their dielectric properties, while others show metallic conductivity, although most are semiconductors. As for other compounds, the electrical behavior in perovskites depends on the outermost electrons, which may be localized at specific atomic sites or may be collective. Since localized electrons may carry a spontaneous moment, there is a strong correlation between the electrical and magnetic properties of perovskites. Rare-earth perovskites containing transition ions show widely differing electrical properties. The electrical properties of perovskites have aroused special interest since the discovery in 1986 of superconductivity at 40 K in cuprates. These cuprates are hole superconductors, exhibiting a mixed valence of copper Cu^{2+}-Cu^{3+}. Among these, the exception is Ce-doped Nd_2CuO_4, with T_c close to 25 K, which belongs to a different structural type and is an electron superconductor. All these compounds have a common feature, the two-dimensional character of the structure, which has been shown to be an important factor for the existence of superconductivity at high temperature [7].

2.2.3 Mixed ionic-electronic conductors

It exhibits both ionic and electronic conductivity for example $La_{1-x}Sr_xBO_{3-\delta}$. When the B ions can take a mixed-valence state, charge neutrality is maintained by both the formations of oxygen vacancies and a change in the valence state of the B ions. The oxides may show both high oxygen ion conductivity due to the high oxygen vacancy concentration, and a high electronic conductivity due to the mixed-valence state [8]. The concentration of oxygen vacancies can also be increased by mild B-site ion substitution, such as Cu and Ni ions, which naturally take the divalent oxidation state [10]. If the valence state of the B ions is fixed, neutrality is maintained only by the formation of oxygen vacancies. The oxides may be predominantly ionic conductors, in this case.

2.3 Perovskite synthesis [11]

2.3.1 Solution reaction

Traditional ways of making perovskite materials usually adopt mixing the constituent oxides, hydroxides and carbonates. However, since these materials generally have a large particle size, this approach frequently requires repeated mixing and extended heating at high temperature to generate a homogeneous and single phase material. In order to overcome the disadvantages of low surface area and limited control of the micro-structure inherent in the high temperature process, precursors generated by sol-gel preparations or coprecipitation of metal ions by precipitating agents such as hydroxide, cyanide, oxalate, carbonate, citrate ions etc., have been used. These gel or coprecipitated precursors can offer molecular or near molecular mixing and provide a reactive environment during the course of subsequent heating and decomposition. Because of the improved solid-state diffusion resulting from the improved mixing, they need a relatively lower temperature to produce similar materials compared to the traditional methods. These methods frequently offer additional advantages, such as better control the stoichiometry and purity, greater flexibility in from thin films and new compositions, and an enhanced ability to control

particle size. Consequently, they have opened new directions for molecular architecture in the synthesis of perovskites.

A convenient way of classifying the methods, which state from solution, is to consider the means used for solvent removal. Two basic classes exist. The first is based upon precipitation with subsequent filtration, centrifugation, etc., used to separate the solid and liquid phases. The second basic method depends upon thermal processes, e.g., evaporation, sublimation, combustion, etc., to remove the solvent. An additional consideration in the latter method is the possible simultaneous conversion of the residue into the desired product. The principal advantages of starting from solution are better homogeneity and improved reactivity. No amount of mixing of solid particles will approach that obtained in solution and most of the other advantages are a direct result of this mixing on essentially an atomic scale. The necessary solid-state reactions proceed more rapidly and at lower temperatures. As a consequence, the desired product can be obtained with a smaller particle size and greater reactivity. Solubility is one of the most important considerations in designing solution techniques. Not only it is desirable that solubility be high in order to minimize the amount of solvent, which must subsequently be removed, but also the particular components must be compatible, e.g., iron sulfates could not be combined with barium chloride in order to produce barium ferrite because barium sulfate would precipitate. Cost, purity and toxicity are other obvious factors. A more subtle concern is the choice of the presumably inert anions, which will be determined by the pH values, ionic strength, degree of super saturation and impurities. This is important firstly because of the tendency of these ions to become incorporated in the final product and secondly because there are subsequent effects can vary dramatically. Conditions that favor large particle size, slow growth and equilibrium will generally produce the purest precipitate.

2.3.2 Solid-state reaction

Conventional processing of the perovskite-related materials uses solid-state reactions between metal-carbonates, hydroxides, and oxides. $BaTiO_3$ represents a typical case. Impurities are introduced from raw materials, milling media, and the calcinations container. Because of the high temperature required for complete

reaction and course, problems such as multiphase have to be minimized in order to generate homogeneous high performance $BaTiO_3$.

2.3.3 Gas phase reaction

The deposition of perovskite films with a specific thickness and composition generally requires gas phase reaction or transport. Many physical techniques have been developed for gas phase deposition such laser ablation, molecular beam epitaxy, dc sputtering, magnetron sputtering, electron beam evaporation and thermal evaporation. In general they can be divided into two categories based on the target they use. The first type uses separate targets where a different speed of deposition for each element has to be determined. The second method uses the performed perovskite material itself as target and the stoichiometric phase is transported to the substrate by sputtering or ablation techniques. Gas depositions can be divided further into three categories: (1) deposition at low substrate temperature followed by a post-annealing at elevated temperatures, (2) deposition at intermediate temperature of 873 to 1073 K, and (3) deposition at crystallization temperature under an appropriate atmosphere.

2.4 Perovskite membrane preparation by solution reaction

2.4.1 Solution reaction synthesis of perovskites

It is well known that the synthesis of ceramic powder by using the conventional method or solid-state synthesis promotes the crystal growth and resulting in a hard agglomeration. The good sinter ability may be achieved when no agglomerated powders are employed or the preparation procedure is such that weak agglomerates are formed. Therefore, the properties of the raw material powder are determined largely by the properties of the raw material powder, on which several requirements are imposed, fine particles (< 1 µm), narrow size range, no aggregation, controlled particle shape, uniformity in chemical and phase compositions, and high purity [12].

Several techniques, especially solution reaction or wet chemical synthesis or liquid phase synthesis, have been developed from solid-state synthesis to produce the required properties of raw powder, such as precipitation [13], freeze drying [14], spray-pyrolysis, sol-gel [15] and liquid mix process, etc. Liquid mix process is a generic name for various processes that start with a homogeneous solution containing the desired cations, which use additives and evaporation to convert the homogeneous liquid to rigid cross-linked polymer, and which utilize heat to convert the polymer into a homogeneous oxide powder. The initial process was pioneered by Pechini and is referred to either as Pechini process [16]. The following steps are used to achieve a powder.

1. An aqueous solution is prepared with metal alkoxides, oxides, hydrated oxides, or carbonates in an alpha-hydroxycarboxylic acid such as citric acid; the ratio of metal ions can be precisely controlled.
2. A polyhydroxy alcohol such as ethylene glycol is added and the liquid is heated to 150 to $250^\circ C$ to allow the chelates to undergo polyesterification.
3. Heating is continued to remove excess water, resulting in solid polymeric resin.
4. The temperature is increased to about $400^\circ C$ to char or decompose the resin.
5. The temperature is further increased to 500 to $900^\circ C$ to form crystallites of the mixed oxide composition. The crystallites are typically 20 to 50 nm and clustered into agglomerates.

The low solubility of Metal oxalates, sulphates, nitrates, chlorides, and acetates in either the liquid or the solid resin is leaded to the phase separation in the final product. Therefore, these metals were avoided to use. A variety of modifications processes for perovskite synthesis have been developed. One was called amorphous citrate process that involves producing precursor from citric acid and metal nitrate before combustion. For production of Sr-substituted $LaMnO_3$ perovskite powder by the amorphous citrate process, the manganese citrate-nitrate precursor may be represented as in Equation 2.2 [17]:

```
    CH₂CO
        \
         \
   C——COO———La
    |     /
    |    O
 CH₂COO
```

(2.2)

(chemical structure diagram of lanthanum and manganese citrate-nitrate complex)
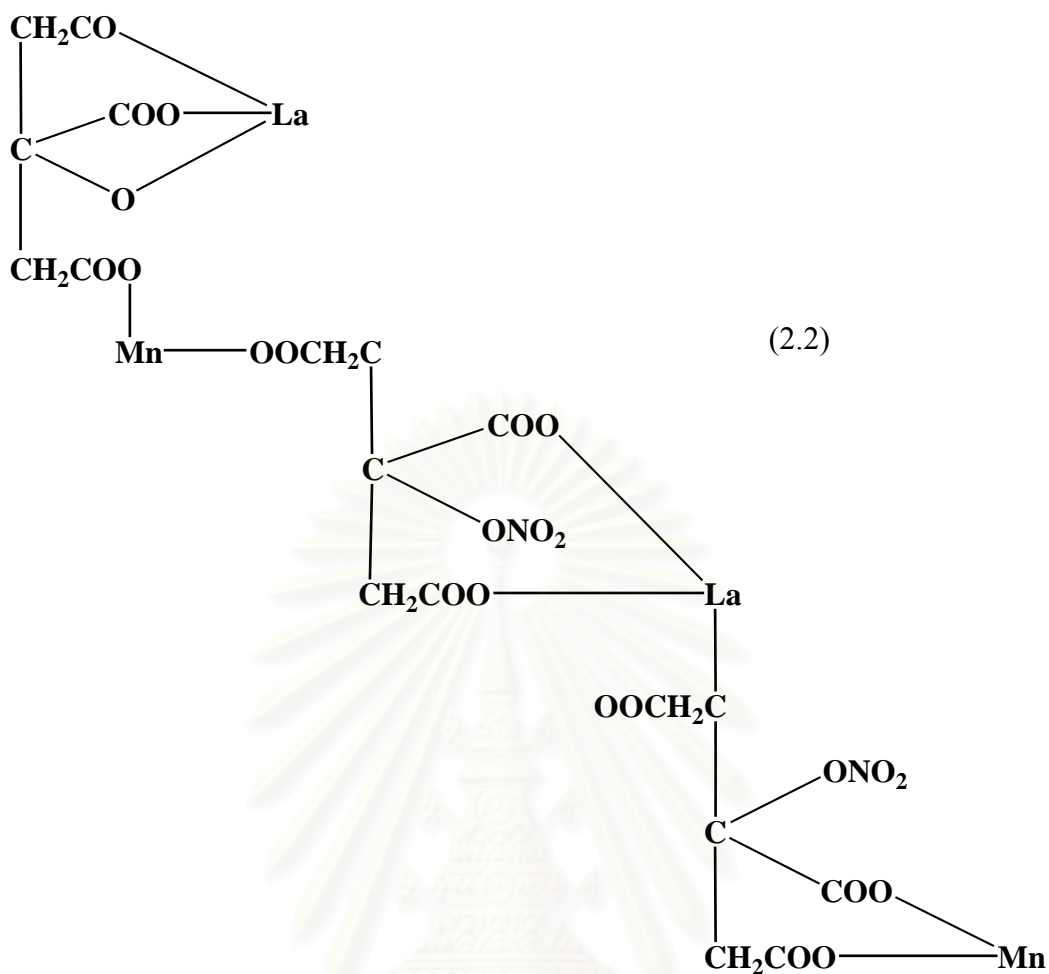
This complex, lanthanum is the trivalent state. It replaces the hydrogen of three –COOH groups in normal citrate formation or one –OH group and two –COOH groups. In the manganese complex, it is the divalent state. Therefore, the two –COOH and one –OH groups were replaced by manganese and NO_2, respectively.

The citric acid pyrolysis method [18] is one of modification of the Pechini processes. This method was used for synthesis of $YBa_2Cu_3O_{7-\delta}$. The first, the mixed metal oxides were dissolved by nitric acid and then adjusted pH value by NH_4OH.

The synthesis method has been developed that involved the use of metal nitrates. One method is called the glycine-nitrate process, uses glycine instead of citric acid [19]. The glycine performs two functions. First, it forms complexes with metals cations and increases their solubility. This seems to prevent selective precipitation and segregation during evaporation. Second, the glycine serves as a fuel during charring. Specifically, metal nitrates are combined with glycine in water and

evaporated until a homogeneous viscous liquid is formed. The liquid is further heated to about 180°C and auto-ignites. Temperatures rapidly reach $1,100^{o}$C to $1,450^{o}$C and nearly instantly convert the material to fine, relatively no agglomerated crystallites of the mixed oxide composition and structure. The glycine nitrate precursor liquid can also be converted to homogeneous mixed oxide powder in a conventional spray drying apparatus.

$La_{0.8}Sr_{0.2}MO_3$ (M = Mn, Co) compounds were synthesized by hydroxy acid-aided process [20]. The mixed aqueous solution of metal nitrates and a hydroxy acid was evaporated and than the compound was generated by calcination in air. The $La_{0.8}Sr_{0.2}MO_3$ perovskites were formed at $550-600^{o}$C but when citric or malic acid was used, the temperature of perovskite formation was $250-300^{o}$C. This temperature is lower than the conventional nitrate process because the malic acid-aided process gave oxides with larger square surface areas. The resulting large surface area oxides are shown excellent catalytic performance for the combustion of methane. The others solution combustion method was developed such as the synthesized $La_{1-x}Sr_xFeO_3$ where x = 0.0-1.0 by Suresh et al. [21]. Oxalyl dihydrazide (ODH) or tetra formal tris azine (TFTA) was used in the reaction. The average agglomerate sizes are 0.89 μm and 4.8 μm for ODH and the TFTA ferrites respectively.

The perovskite compounds that were synthesized by wet chemical methods give the very fine compound and no agglomerated that facilitates the densification. The sintering temperature of perovskite that synthesized in this method can be used at lower than for those synthesized by conventional solid-state methods.

Liquid mix process is distinguished when comparing in several wet chemical techniques such as less energy consumption, simplest technology, and potential to get fine particles and a single phase powder. Both adding several acids such as citric, malic acid, or etc. and adjusting the pH of aqueous solution are used to provide the fine homogeneous perovskite with the high surface area.

2.4.2 Powder sizing

A range of particle size is required to achieve maximum particle packing because the compacting and sintering are depended on particle size. The ball milling is the common techniques to achieve the desire particle size of powder.

The objective of pressing step is to improve particle packing and uniformity. Therefore, minimum shrinkage and retained porosity will result during densification. The hardness and density of agglomerates in ceramic compound is resulted from the large interagglomerate after sintering. Therefore small particle size is required because it facilitates the high strength of green disc. The small particle can be compacted into a porous shape and sintered at a high temperature to near-theoretical density [22].

Calcined powder is not usually available with the optimum particle size distribution. The ball milling and screening are the common techniques to achieve the desire particle size of powder.

2.4.3 Powder compacting by uniaxial pressing [22, 12]

Placing the powder into a rigid die and applying pressure along a single axial direction through a rigid plunger, or piston to achieve compacting accomplish uniaxial pressing. Pressing results in the direct contact of particles, reduces the average distance between particles, and changes the shape of particles. The apparent density of a compact was controlled by mixing of the proper various particles size fractions.

To enhance the compacting, before pressing, the powder should be disaggregated by mixing the powder with solvent such as isopropanol in the ultrasonic bath or added a couple drops of acetone to reduce the surface tension.

2.4.4 Sintering [23]

Sintering is a process of permanent chemical and physical change by the decreasing of porosity by the grain growth and grain bonding at high temperature. When an aggregated powder is sintered, necks of interagglomerate are formed between the particles, and the density of aggregate is increased. The growth of the neck is increased with the transport of matter or the counter-flow of vacancies between the particles and the pores. The sintering can be classified into three stages. The first stage or initial stages during which the necks form at points of particle contact and the particles usually center approach each other. At this stage the individual particles are still distinguishable. The second stage or intermediate stage during that the necks become large, resulting in the formation of an interconnected pore structure. The third or the final stage during, the pore becomes isolated. The interconnectivity of pores was eliminated affected to eliminate of surface and vapor transport [24].
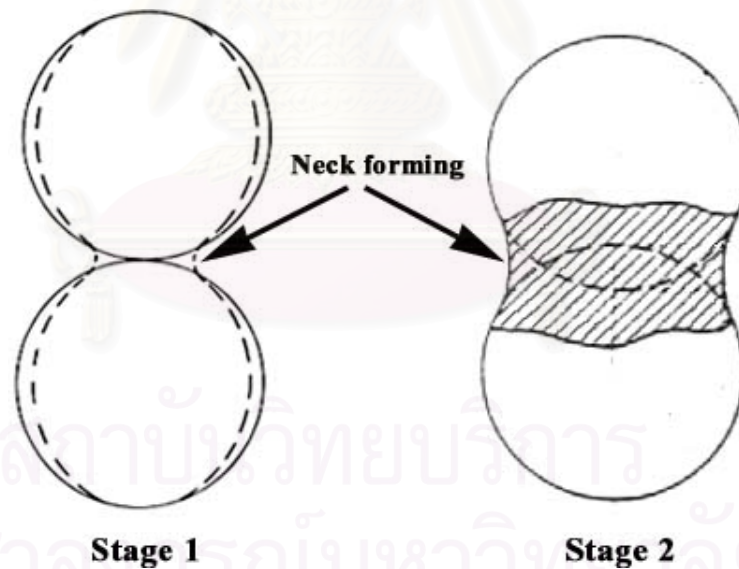
Figure 2.2 Mechanism of sintering.

2.5 Dense perovskite membranes for oxygen separation

2.5.1 Perovskite membrane concepts [25]

The use of perovskite membrane reactor technology under development for the spontaneous conversion of natural gas to synthesis gas has important commercial implications. Because the perovskite membrane reactor process is exothermic and eliminates the need for a separate oxygen plant, a reduction in synthesis gas production costs may be realized. Additionally, NO_x emissions are eliminated since atmospheric nitrogen is excluded from mediating through the membrane. These dense perovskite membranes are exclusive oxygen anion conductors with oxygen anion transport proceeding from reducing to oxidizing membrane surfaces with electrons mediating from oxidizing to reducing surfaces via the membrane lattice bulk. A principle behind application of this perovskite membrane reactor technology for the spontaneous conversion of natural gas into synthesis gas is shown in Figure 2.3. These devices behave as short-circuited electrochemical cells, except that no electrical energy is required to drive this thermodynamically downhill process.
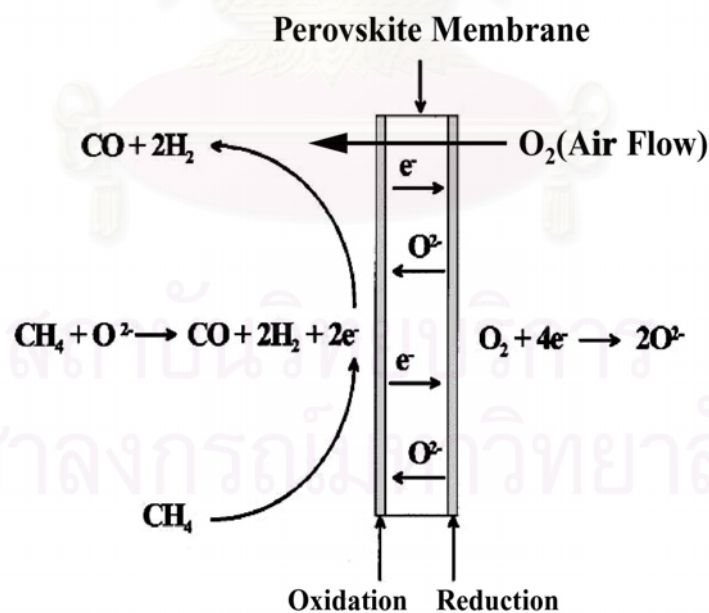
Figure 2.3 Perovskite membrane concepts.

Current commercially available technology for synthesis gas production from natural gas is based on the endothermic steam reforming reaction, which may be represented by:

$$CH_4 + H_2O \longrightarrow 3H_2 + CO \qquad (2.3)$$

With CO also reacting with water via the water–gas shift reaction:

$$CO + H_2O \longrightarrow CO_2 + H_2 \qquad (2.4)$$

In contrast, the methane partial oxidation reaction:

$$2CH_4 + O_2 \longrightarrow 2CO + 4H_2 \qquad (2.5)$$
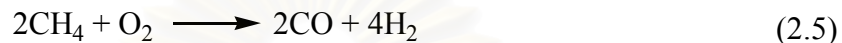
Proceeding across mixed oxygen anion and electron-conducting membranes is exothermic, with oxygen being separated from the atmosphere at the membrane reducing surface for subsequent participation in the natural gas partial oxidative reforming reaction at the membrane oxidizing surface. The two formidable technical problems controlling development of perovskite membrane reactor technology for achieving the spontaneous partial oxidation of natural gas into synthesis gas have been (1) the ability to mediate a sufficiently high flux of oxygen across the membrane and (2) achieving this for materials which possess high stability perovskite membrane must be simultaneously stable to natural gas on the partial oxidation surface and air at their reducing surface, all at $900^{\circ}C$.

2.5.2 Oxygen permeation through a mixed-conducting membrane [26]

There are 5 steps for oxygen to permeate through an ion-conducting membrane from side A with high oxygen pressure to side B with low oxygen pressure. As shown in Figure 2.4, firstly gas-solid mass transfers of gaseous oxygen (Steps 1 and 5) and then surface exchange between molecular oxygen and oxygen vacancies (Steps 2 and 4) and the oxygen vacancy bulk diffusion (Step 3). Under certain conditions such as small membrane thickness, high ionic conductivity and/or fast surface exchange rates, gas-solid mass transfer may exert a partial control over the oxygen permeation rate across the membrane. Based on experimental investigation, gas-solid mass transfer does not significantly influence the oxygen permeation under conditions concerned and thus has been eliminated as a rate-

controlling factor. Therefore, the permeation analysis in this section focuses on surface exchanges (Steps 2 and 4) and bulk diffusion (Step 3). In this case, the interfacial oxygen partial pressures ($P'_{O2,i}$ and $P''_{O2,i}$) are equal to the main stream pressures (P'_{O2} and P''_{O2}) respectively, for each side.
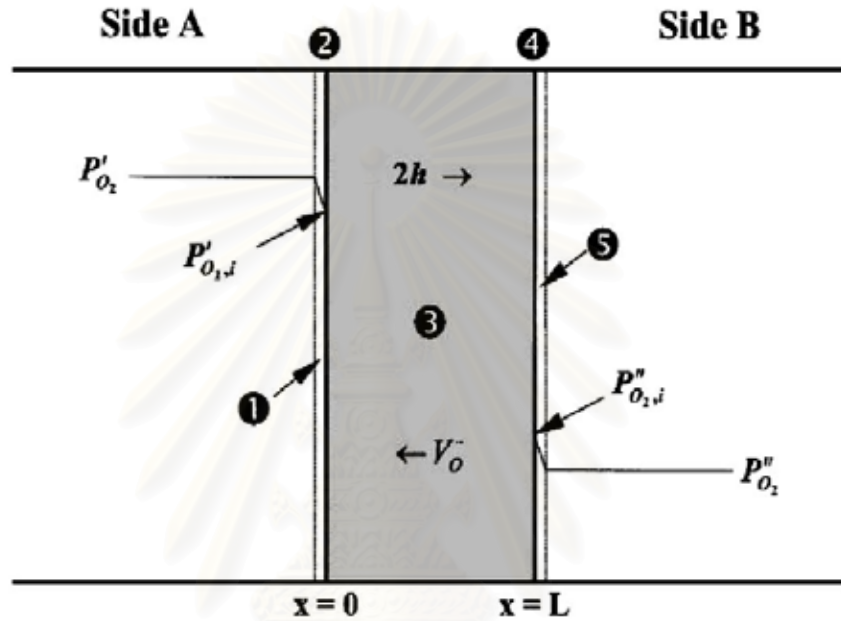
Figure 2.4 Oxygen permeates through an ion-conducting membrane.
(Assuming that oxygen vacancies, $V\ddot{o}_2$; electron-holes, h and membrane thickness, L)

At the steady-state oxygen permeation flux can be readily correlated to P'_{O2} and P''_{O2} in an explicit equation [27].

$$J_{O_2} = \frac{D_V k_r (P'^{0.5}_{O_2} - P''^{0.5}_{O_2})}{2Lk_f (P'_{O_2}P''_{O_2})^{0.5} + D_V(P'^{0.5}_{O_2} + P''^{0.5}_{O_2})} \qquad (2.6)$$

Where D_v, k_r and k_f are functions of temperature and the specific properties of the membrane and can be determined by fitting experimental oxygen flux data as a function of temperatures and oxygen partial pressure gradients.

2.6 Profiles of perovskite membrane reactor for oxygen separation

2.6.1 Tubular membrane reactor [28]

2.6.1.1 Sealing of tubular membranes

Three sealants including a $Cu(OH)_2$ binder, a Pyrex glass ring, and a ceramic binder were studied in detail in order to find the best one. The $Cu(OH)_2$ binder was used together with phosphoric acid. The ceramic binder contains extra-fine alumina and some of the prepared perovskite type oxide. As will be indicated in the subsequent section, the ceramic binder was found to be best and was used for oxygen permeation measurement.

2.6.1.2 Tubular membrane reactor setup

A tubular membrane separator shown in Figure 2.5 was used for the measurement of oxygen permeation. Two dense alumina tubes supported the tubular dense membrane. The ceramic binder was used to seal both ends of the membrane with the walls of these alumina tubes. A quartz tube surrounding the two-alumina tubes formed the shell side of the separator, which was surrounded by a tubular furnace, and the temperature was measured by a type K thermocouple encased in an alumina tube. A microprocessor temperature controller was used to control the temperature to within ($1^{o}C$ of the set points). The oxygen permeation rates through the dense tubular membranes were measured on the permeation apparatus given in previous study [29]. Air was introduced into the shell side of the tubular membrane. Helium as the sweep gas was fed to the tube side of the tubular membrane. Both upstream and downstream were maintained at atmospheric pressure. The effluent streams were analyzed by a gas chromatograph. The amount of oxygen passing through the membrane was calculated from the flow rate and the oxygen concentrations of the effluents.
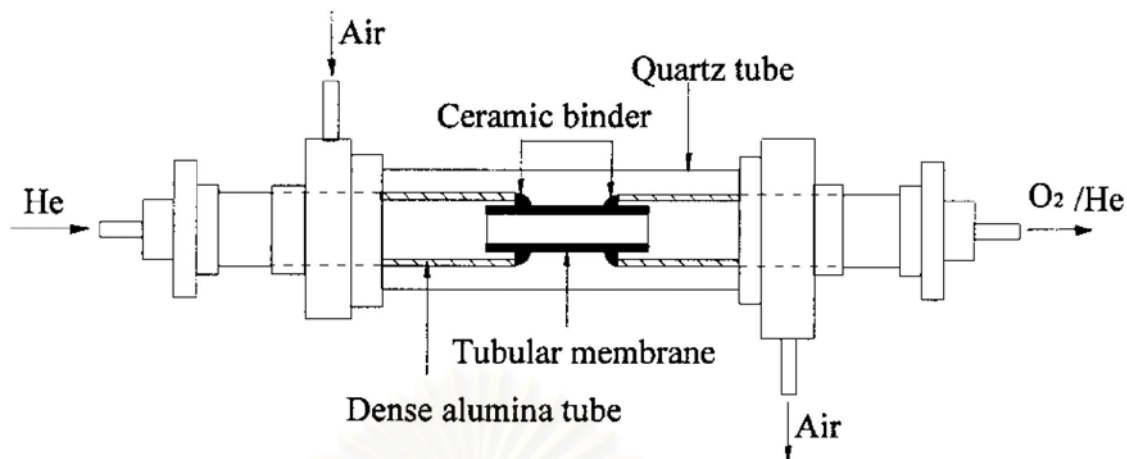
Figure 2.5 Tubular membrane separators

2.6.2 Disc-shaped membrane reactor

2.6.2.1 Sealing of disc-shaped membranes

The process of mounting a perovskite disc to a quartz tube has been developed. To separate oxygen from the air, the joint material has to be able to form an airtight bond with quartz and with perovskite, and to accommodate the thermal expansion mismatch between quartz and perovskite. It also has to be inert in an air and methane environment, and has a high melting or softening point, that can be specially applied to the high temperature partial oxidation of methane to syngas reaction. Gold, the most ductile element with a melting point of $1064^{o}C$ and inertness for most chemical reactions fulfills the criteria mentioned above.

De Bruin et al [30] studied the mechanisms of noble metals and transition metals bonding on the ceramics. They showed a vacuum-tight bond between gold and Pyrex glass. Bailey and Black described the methods for fabrication of some strong vacuum-tight bonds between gold and alumina [31]. Those methods were modified as follows: pure Au foils was cut into rings. They were then cold-rolled to ensure flatness on the surface. A one-foot-long quartz tube with an extremely flat end was fire polished to remove the loosened grains. The sintered perovskite discs were hand-polished by using carbide papers. The extra low-lint wiper was used to clean the

surfaces of the discs. If needed, a re sintering process would be applied to the perovskite discs.

2.6.2.2 Disc-shaped membrane reactor setup

Air used as without further purification. Helium flowed through an adsorptive oxygen trap to remove oxygen and moisture before being introduced to the system. The experimental layout is shown in Figure 2.6. Flow controller calibrated by a bubble flow meter regulated the flow of gases into the reactor. An electronic pressure transducer was used to accurately detect the reactor pressure, and a backpressure regulator was used to maintain the feed-side pressure to 780 mm Hg. A programmable temperature controller controlled a pre-calibrated vertical three-section furnace with thermocouple, allowing the reaction zone to be operated isothermally or in a temperature-programmed mode.

Details of membrane reactor design are shown in Figure 2.7. A sintered disc was polished to the thickness of interest and then mounted on a quartz tube using a gold ring seal. It was important to keep the clearance as small as possible to reduce the possible dead volume.

Before turning on the air, helium was flushed through the permeate side of the reactor until air was completely replaced. One side of the membrane disc was exposed to air (180 cm^3/min), while the other side was exposed to pure helium ($\sim$ 30 cm^3/min) in the permeation runs. The permeated gases were analyzed by on-line gas chromatography.
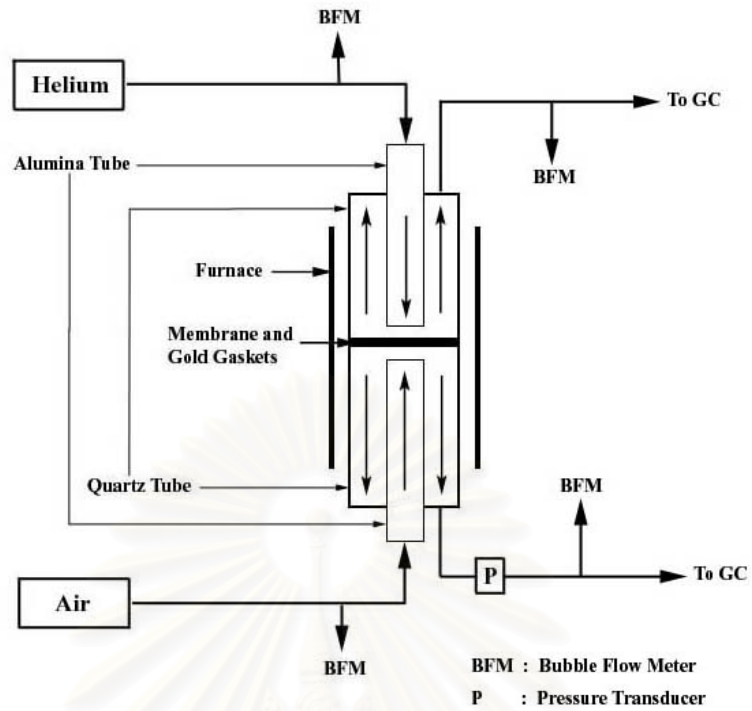
Figure 2.6 A disc-shaped membrane reactor layout
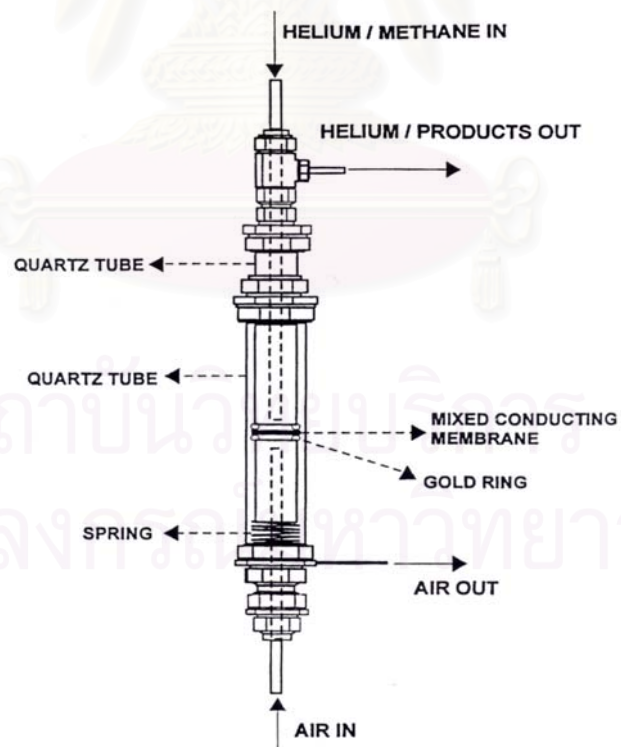
Figure 2.7 A disc-shaped membrane reactor

2.6.3 Coated disc membrane reactor

Ishihara et al. [32] applied the mixed ion conductor of $La_{0.7}Sr_{0.3}Ga_{0.6}Fe_{0.4}O_3$ for the oxygen permeating membrane for CH_4 partial oxidation. The powder of $La_{0.7}Sr_{0.3}Ga_{0.6}Fe_{0.4}O_3$ after calcination was pressed into a disk. The obtained disk was painted on both surfaces with $La_{0.6}Sr_{0.4}CoO_3$ (LSC) slurry (30 mg and 40 μm thickness) at 10 mm in diameter with screen-printing method in order to improve the surface activity for oxygen dissociation. LSC was prepared by calcinations of the mixture of $La(NO_3)_3$, $Sr(NO_3)_2$, and $(CH_3 COO)_2Co$ at 1273 K for 6 h. Permeating oxygen from air to He was analyzed with a gas chromatograph. For the partial oxidation of CH_4, Ni and LSC were mainly coated on the membrane as partial oxidation and oxygen dissociation catalyst, respectively. Coating of the catalyst was performed with the screen-printing method and 30 mg of each catalyst was applied at 40 μm in thickness. For the deposition of metal catalyst, NiO, $PdCl_2$, $RuCl_2$, $RhCl_2$, CoO, and Fe_2O_3 were coated as a precursor and the coated precursor was reduced to metal by feeding H_2 (50 ml/min) at 1273 K, 1 h before reaction. Methane diluted with N_2 ($CH_4:N_2 = 2:1$) was fed at 50 ml/min for a reactant and dry air at 100 ml/min for oxidant. Molten Pyrex glass was used for sealing gas as shown in Figure 2.8. All products were analyzed with the gas chromatograph.
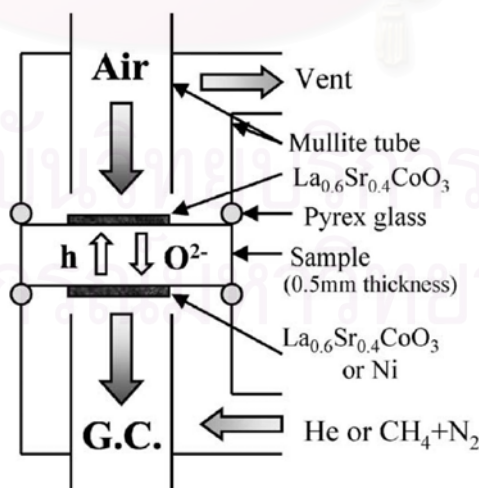
Figure 2.8 Coated disc membrane reactor.

CHAPTER 3

LITERATURE REVIEW

Mixed oxide ionic and electronic conducting membranes have been studied widely for application in oxygen separation [33] such as oxygen sensors [34], solid oxide fuel cells [35, 36], the partial oxidation of methane to syngas [37] and the partial oxidation of ethane to syngas [38]. Among them, perovskite-type ceramic membranes exhibit the highest oxygen permeability due to their high ionic and electronic conductivity. They were held great promise for applications in separating oxygen from air and improving the performance of catalytic partial oxidation of hydrocarbons [39]. Much research has been directed towards developing materials with high oxygen permeation flux, and good stability at high temperatures and reducing conditions. However, the performance of perovskite membranes can be affected by many factors such as type, methodology of synthesis, composition, membrane thickness, microstructure and temperature at which the membranes are to be used [40].

3.1 Perovskite based oxide types LaGaO$_3$

There is an attempt to find new materials giving high oxygen permeation flux and good stability for preparation the oxygen separating membrane. In recent years, LaGaO$_3$ based perovskite has been considered as a membrane to separate oxygen from air [41]. Since it exhibits high O^{2-} permeation at high temperatures, and the structure of this composition is very tolerant to the incorporation of foreign cations and a large number of cations can be used to partially substitute for either La or Ga [42].

Lybye et al. [43] compared the conductivity of LaAlO$_3$, LaGaO$_3$, LaInO$_3$ and LaScO$_3$ perovskites with doped 10% Sr on A-site and 10% Mg on B-site. They found that doped LaGaO$_3$ exhibits high oxide ion conductivity. It is suggested that the high conductivity of doped LaGaO$_3$ in a cubic perovskite, A-cations and oxide ions form a cubic are close-packed structure to avoid strains in the lattice and B cation has to fit

on the octahedral space. The optimum size of B can be calculated from the tolerance factor. When La was used as A-site cation, r is 0.56 $\overset{o}{A}$. This means that aluminum is too small, gallium is slightly too big, and scandium and indium are far too big (see the ionic radii in Appendix A) due to the introduction of the oxygen vacancies, the B-site ion should be about 10% bigger in order to minimize the strain if the analogy from the fluorites is used. This means $r \approx 0.6$ $\overset{o}{A}$, which is close to the radius of Ga. La on the A-site is the optimal ion as La^{3+} has the ionic radius closest to the radius of O^{2-}. Therefore La^{3+} and Ga^{3+} have the ionic radii closest to the ideal ionic radii necessary to obtain the ideal strain-free perovskite lattice, where oxide ions can move easily. Consequently, it is concluded that doped LaGaO$_3$ exhibits highest oxide ion conductivity.

3.1.1 Effect of A-site substitution on LaGaO$_3$ based perovskite

Teraoka et al. [44] reported some perovskite-type oxides containing transition metals at B site show high electrical conductivity. The partial substitution of A-site cations by other metal cations with lower valences often brings about the formation of oxygen vacancies affects to produce the ionic conduction. The rate of oxygen permeation through La$_{1-x}$Sr$_x$Co$_{1-y}$Fe$_y$O$_{3-\delta}$ was found to increase with an increase in Sr or Co content. It is shown that the permeability was mainly controlled by the amount of oxygen vacancies.

Ishihara et al. [42] also informed that the Sr substitution increased the electrical and ionic conductivity of the LaGaO$_3$ based perovskite, as compared to the undoped. It was mentioned that the ionic conductivity, σ_i, increased with an increase in the amount of Sr additives and attained the maximum limit of the solid solution at x = 0.1 in La$_{1-x}$Sr$_x$GaO$_{3-\delta}$.

In addition, Li et al. [45] confirmed that by comparing the oxygen permeability of La$_{0.2}$A$_{0.8}$Co$_{0.2}$Fe$_{0.8}$O$_{3-\delta}$ (A = Sr, Ba and Ca) membranes. Perovskite membranes were prepared by the solid-state method with desired properties and high oxygen permeation flux. The activation energies for oxygen permeation of

$La_{0.2}A_{0.8}Co_{0.2}Fe_{0.8}O_{3-\delta}$ (A = Sr, Ba and Ca) membranes are 106.4, 123.3 and 144.0 kJ/mol, respectively are shown in Figure 3.1 and Table 3.1.

Therefore, Sr-substitution compound has the highest oxygen permeation fluxes because of the lower average bond energy, highest free volume, and largest critical radius. And the substitution of La^{3+} by Sr^{2+} was compensated by the promotion state and/or by the formation of oxygen ion vacancies. Consequently, the oxide ion conductivity was increased.
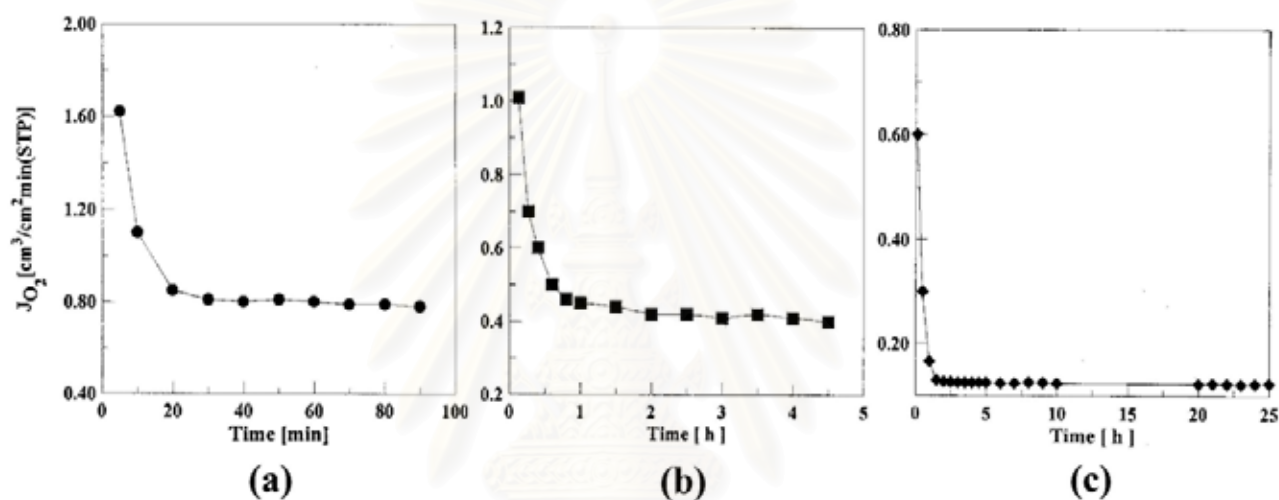
Figure 3.1 Transient process of oxygen permeation through perovskite-type membranes at $1173^{o}K$ (a) $La_{0.2}Sr_{0.8}Co_{0.2}Fe_{0.8}O_{3-\delta}$, (b) $La_{0.2}Ba_{0.8}Co_{0.2}Fe_{0.8}O_{3-\delta}$ and (c) $La_{0.2}Ca_{0.8}Co_{0.2}Fe_{0.8}O_{3-\delta}$.

Table 3.1 Oxygen permeation properties of perovskite membranes

Membrane	Equilibration time (min)	Steady state J_{O_2} (950 ^{o}C)* (cm^3/cm^2 min)	E_a (kJ/mol)
$La_{0.2}Sr_{0.8}Co_{0.2}Fe_{0.8}O_{3-\delta}$	20	0.81	106.0
$La_{0.2}Ba_{0.8}Co_{0.2}Fe_{0.8}O_{3-\delta}$	40	0.40	123.3
$La_{0.2}Ca_{0.8}Co_{0.2}Fe_{0.8}O_{3-\delta}$	120	0.12	144.0

* Oxygen partial pressure, 0.21/1 x 10^{-3} atm; helium flow rate, 30 ml/min.

According to these reports, it is concluded that Sr is the most suitable dopant for A-site of $LaGaO_3$.

3.1.2 Effect of B-site substitution on $LaGaO_3$ based perovskite

Gharbage et al. [46] estimated the holes conductivity of lanthanum gallate-based samples ($La_{0.9}Sr_{0.1}Ga_{1-x}Fe_xO_{3-\delta}$, with $x = 0$ and $x = 0.2$), in the range 700–1,000^{o}C. These estimates were based on electrochemical permeability measurements, and were compared to previous estimates obtained from ion-blocking measurements (Figure 3.2).
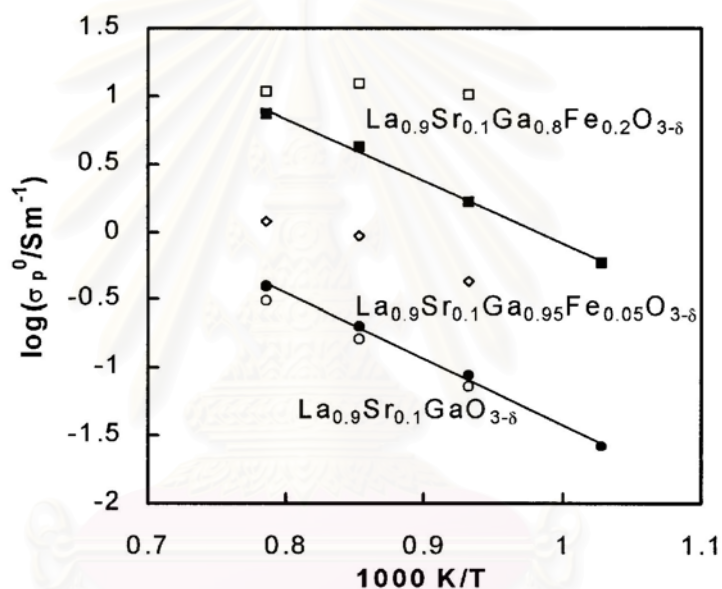
Figure 3.2 Arrhenius-type plots for electrical conductivity, σ_p^{o} of Fe-free and doped samples (closed symbols). Also included are values previously obtained by ion-blocking measurements (open symbols)

The electrical conductivity of these materials was strongly influenced by the content of Fe. The activation energy for electrical conductivity was found to be in the range 0.9–1 eV, lower than usually observed for alternative electrolytes based on zirconia or ceria. The increase in electrical conductivity with Fe content can be explained by a relatively easy formation of Fe^{4+} ions under oxidizing conditions, a basic requirement for the establishment of a small polaron-type conduction mechanism. Ishihara et al. [47] confirmed that Fe is the suitable dopant for Ga site.

Mixed electronic–oxide ionic conductivity in $LaGaO_3$ -based oxide doped with Fe, Co or Ni was investigated in this study. The electric conductivity was greatly increased by doping Fe, Co, or Ni for the Ga site of $La_{0.8}Sr_{0.2}GaO_{3-\delta}$. Compared to the conventional mixed electronic–ionic conductors such as $LaCoO_3$, these $LaGaO_3$ - based oxides exhibited a lower electronic conductivity but higher oxide ion conductivity. In particular, Fe-doped $LaGaO_3$ exhibited a highest oxygen permeation rate (Figure 3.3) and stability against reduction at 1,000-1,200 K that is the range of partial oxidation processing temperature. Moreover, using $La_{0.8}Sr_{0.2}Ga_{0.6}Fe_{0.4}O_3$ attained higher CH_4 conversion in the partial oxidation of CH_4.
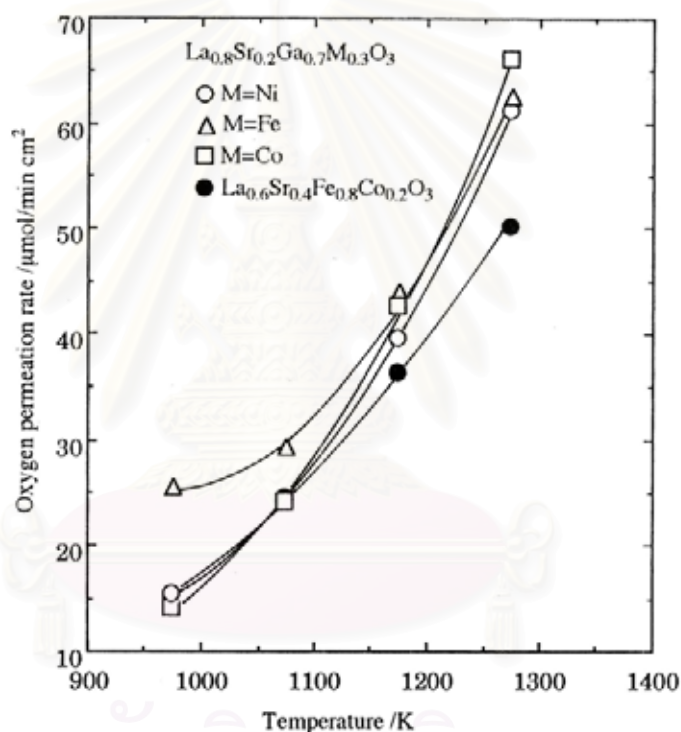
Figure 3.3 Temperature dependence of oxygen permeation rate

For the both of A-site and B-site substituted on $LaGaO_3$, Ming et al. [48] revealed the XRD patterns of $La_{0.5}Sr_{0.5}Ga_{0.2}Fe_{0.8}O_{3-\delta}$ perovskite oxide in a reducing environment (22% CH_4 + 57% H_2 + 21% CO_2) which showed the perovskite oxide remained cubic over the temperature range of 20 to $800^{\circ}C$ (Figure 3.4). At $1,000^{\circ}C$, $La_{0.5}Sr_{0.5}Ga_{0.2}Fe_{0.8}O_{3-\delta}$ underwent decomposition, associated with the disappearance of the strongest peak and the appearance of two new peaks around the original position (2θ about 32°). XRD patterns between 800 and $900^{\circ}C$ as displayed in Figure

3.5, indicated that the decomposition of LSGFO occurred at 860°C. A good match of these new peaks with the expected (LaSr)GaO$_3$ and iron peaks allowing for shifts due to thermal expansion indicated that the decomposition products were (LaSr)GaO$_3$ and iron. The decomposition of La$_{0.5}$Sr$_{0.5}$Ga$_{0.2}$Fe$_{0.8}$O$_{3-\delta}$ is due to the highly reducing environment. It was reported that the parent structure LaFeO$_3$ was stable at an oxygen partial pressure of 10^{-17} atm and temperatures below 1,000^{o}C. They found that Sr and Ga substituted LaFeO$_3$ underwent a decomposition at an oxygen partial pressure of 10^{-17} atm at 860°C.
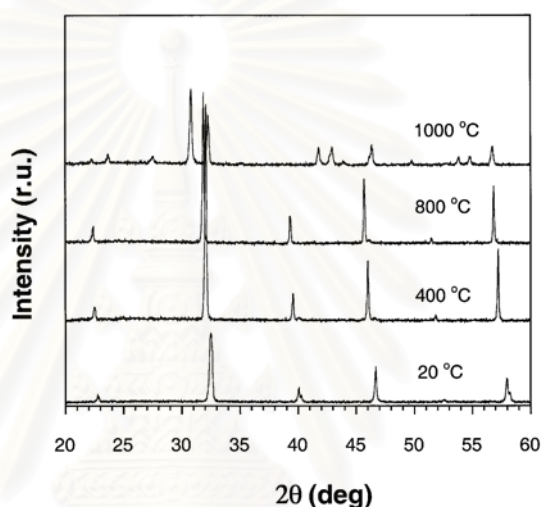
Figure 3.4 XRD patterns of La$_{0.5}$Sr$_{0.5}$Ga$_{0.2}$Fe$_{0.8}$O$_{3-\delta}$ at different temperatures in syngas environment.
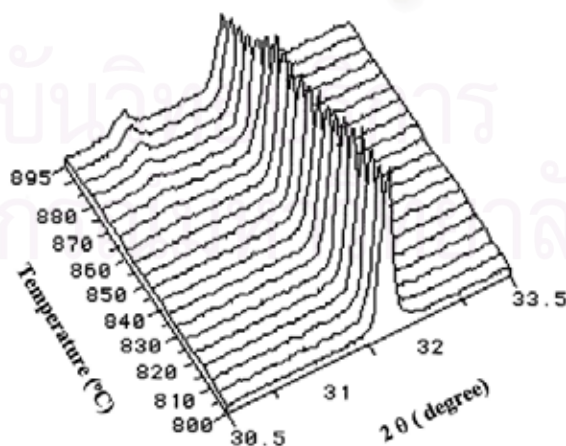
Figure 3.5 XRD patterns of La$_{0.5}$Sr$_{0.5}$Ga$_{0.2}$Fe$_{0.8}$O$_{3-\delta}$ during continuous temperature scan.

The perovskite $La_{0.5}Sr_{0.5}Ga_{0.2}Fe_{0.8}O_{3-\delta}$ was reported to have a higher oxygen permeation rate than the non-perovskite oxide, $SrFeCo_{0.5}O_{3-\delta}$ [49]. Materials studied containing cobalt on the B site is normally not stable at low oxygen partial pressures. Iron based systems, in contrast, are more stable than cobalt compounds.

Accordingly, this several research revealed that $LaGaO_3$-based oxide doped with Sr and Fe could be a suitable material for an oxygen permeation membrane, in particular, for air separation in the methane partial oxidation process.

3.2 Effect of pH on the perovskite synthesis by modified method [6]

Figure 3.6 shows the XRD patterns of the LSGF 6428 samples. The results show that a single phase $LaGaO_3$ perovskite was obtained in all powder except pH = 1.10. It should be noted that all solutions were clear except at pH = 3.39. At this pH, the precipitation may be due to the polymerization of metal citrate-nitrate complex, which occurred and did not disappear during the combustion process. However, the obtained powder still is the single phase. This might be due to the fact that, with the sufficient NH_4NO_3, this powder could crystallize at the spontaneous combustion temperature. The powders after the spontaneous combustion were then ground by using a mortar and a pestle both before and after calcination at $900^{o}C$ for 5 hours.
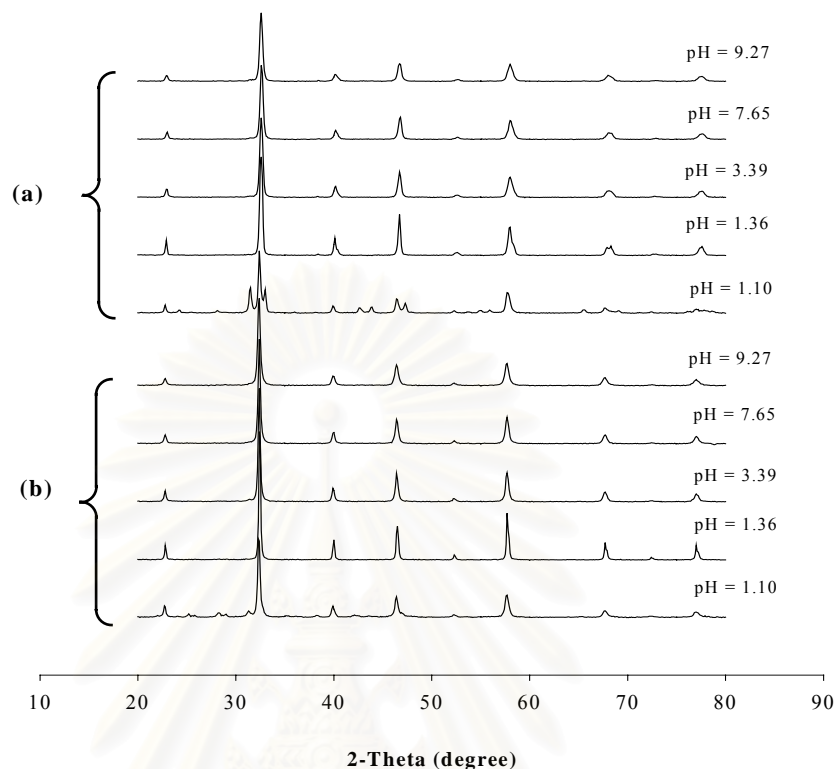
Figure 3.6 XRD patterns of $La_{0.6}Sr_{0.4}Ga_{0.2}Fe_{0.8}O_{3-\delta}$ at different pH (a) calcination at 900^oC and (b) without calcination.

XRD patterns of $La_{0.6}Sr_{0.4}Ga_{0.2}Fe_{0.8}O_{3-\delta}$ at pH = 1.10 showed that the secondary phase of $SrLaGaO_4$ existed in both the uncalcined powder and the powder calcined at 900^oC. It was possible that at pH = 1.10 the amount of the NH_4NO_3 for initiating the combustion was not sufficient to develop the high flame temperature. Generally, the combustion involves two components, fuel and oxidant (normally air), which are heated to the suitable circumstance [50]. If there was sufficient amount of fuel, the combustion tended to give the high rate of flame propagation leading to the high temperature of the flame and less combustion time. Therefore, at pH = 1.10, the spontaneous combustion might have taken place at a low rate, resulting in the longer spontaneous combustion.

3.3 Effect of temperature on crystal structure development [40]

Tan et al. investigated the development of crystal structure of $Ba_{0.5}Sr_{0.5}Co_{0.8}Fe_{0.2}O_{3-\delta}$ perovskite powders synthesized by solid-state reaction method and modified citrate method. DSC curves of powders was shown in Figure 3.7
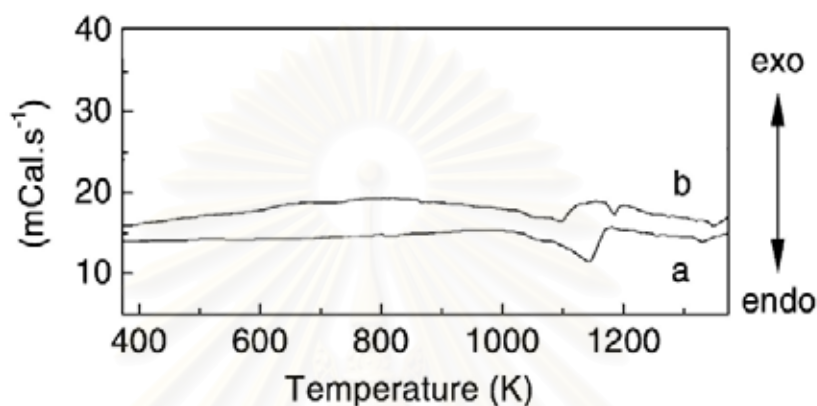
Figure 3.7 DSC curves of BSCF powders after heated at 473K synthesized by solid-state reaction method (a), modified citrate method (b)

The existence of the two peaks in the DSC curves of the powders synthesized by the modified citrate method is shown in Figure 3.7b. A two-step process of the formation of perovskite phase may be suggested, in which the perovskite phase primarily forms in the first step and the disappearance of the miscellaneous peaks occurs in the second step. It also can be concluded from the temperatures at which the peaks exist in Figures 3.7a and b. The formation of the perovskite phase in the powders synthesized by the modified citrate method is earlier than that in the powders synthesized by the solid-state reaction method, and the order of the temperature for complete development is on the contrariness. This is further verified by the XRD patterns of the powders calcined at 1173 K, in which more miscellaneous peaks exist for the powders synthesized by the modified citrate method. From the heights of the peaks, powders synthesized by the modified citrate method need less energy for crystal transformation than those formed from the solid-state reaction. Kwon et al. [51] also pointed out that the thermal energy released in flash-decomposition might induce the nucleation for the perovskite phase formation, so that the energy needed for complete transformation is less.

3.4 Effect of material compositions on sintering property

Kleveland et al. [52] synthesized $La_{1-x}M_xCoO_{3-\delta}$ (M = Ca, Sr; x = 0.2) by glycine-nitrate and EDTA methods. They found that the sintering temperature is decreased in the order $LaCoO_3$ > 20% Sr > 20%Ca. Therefore, the controlling of the composition of $LaCoO_3$ is important for dense materials.

Mori et al. [53] reported that La_xCrO_3 with x > 1.0 showed the orthorhombic and rhombohedral structure for $LaCrO_3$ and Cr_2O_3, respectively. Moreover, La_xCrO_3 samples with x ≥ 1.02 were not stable in air, because La_2O_3 in the samples can react with moisture and form $La(OH)_3$. The formation of $La(OH)_3$ causes a volume change, the samples broke down.

Mori et al. [54] further investigated the sintering behavior of $La_{1-x}AE_xCrO_3$ (AE = Ca and Sr), 0 ≤ x ≤ 0.3. They found that the density of both perovskites is increased with the decreasing AE content. Moreover, they reported that when x ≤ 0.2, the sintering properties of $La_{1-x}Ca_xCrO_3$ are lower than $La_{1-x}Sr_xCrO_3$, but at x = 0.3 the result is reversed.

Stevenson et al. [41] synthesized the lanthanum gallate ($LaGaO_3$) doped with Sr and Mg by combustion synthesis technique. They found that Ga_2O is loss in sintering temperature around 1,400 to 1,600^{o}C. This phenomenon is possibly due to the volatilization of Ga_2O from the perovskite structure as shown in Equation 3.2.

$$Ga_2O_3 \text{ (s)} \quad \leftrightarrow \quad Ga_2O \text{ (g)} + O_2 \text{ (g)} \qquad (3.2)$$
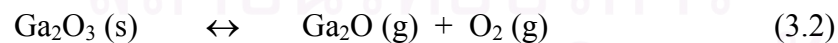
Khanlou et al. [55] studied the microstructure of the compound $La_{0.8}Sr_{0.2}Ga_{0.9+x}Mg_{0.1}O_{3-\delta}$ (-0.02 < x < 0.04) on the sintering behavior. They found that $LaSrGa_3O_7$, $SrLaGaO_4$, and La_2O_3 appeared with increasing sintering temperature.

Therefore, several factors affecting the Ga vaporization in the doped LaGaO$_3$ such as the sintering temperature and composition of dopant that should be further studied.

CHAPTER 4

EXPERIMENTAL

The comprisal of perovskite compounds synthesis, perovskite membranes preparation and characterization of materials, are described as below:

4.1 Chemicals

The chemicals listed in Table 4.1, were used without further purification.

Table 4.1 Reagents for synthesis of perovskite

Reagents	Formula Weight	Purity%	Company
$La(NO_3)_3 \cdot 6H_2O$	433.02	99.999	Aldrich
$Sr(NO_3)_2$	211.63	99.995	Aldrich
$Fe(NO_3)_3 \cdot 9H_2O$	404.00	99.99+	Aldrich
$Ga(NO_3)_3$	255.74	99.999	Alfa
Citric Acid	192.12	99.5+	Aldrich
HNO_3	63.01	70	Lab-Scan
NH_4OH	35.05	30	Panreac

4.2 Synthesis of perovskite compound by modified citrate method

The compound preparation was modified from the citrate pyrolysis method [27]. Stoichiometric amounts of corresponding high purity metal nitrates (based on 0.02 mole of perovskite) in each composition as shown in Table 4.2 were partially dissolved in 10 ml of nitric acid (70%). Then citric acid with an amount of two times of the total metal ions was added. The mixture solution was then titrated with NH_4OH at the controlled rate of 2-3 ml/min. The pH of the solution was adjusted to 7-9. Then the solution changed from partially dissolved brown solution to clear brown solution. To prepare a basic homogeneous solution, a further NH_4OH titration (5 ml) was necessary after most of the metal nitrates were dissolved.

The combustion of the homogeneous solution was carried out on a hot plate at around $200^{\circ}C$ in a three-liter beaker covered with a fine sieve to prevent the loss of fine compounds. The water was evaporated until a sticky gel was obtained. Then it became a large swelling viscous mass and finally self ignited by NH_4NO_3. The combustion lasted for about 10-20 seconds. The sponge-like solids expanded to occupy almost 2/3 of the beaker volume at the end. The resulting compound was ground in a mortar with a pestle, and then calcined in the air at $800^{\circ}C$ for 4 hours with heating rate of $2^{\circ}C/min$ to achieve phase purity or reduce the residual carbon. The particle was ground completely well by mortar before characterization.

Table 4.2 Stoichiometric amounts of metal nitrates based on 0.02 mole of perovskite

Composition	Amounts of metal nitrates (g)			
	$La(NO_3)_3 \cdot 6H_2O$	$Sr(NO_3)_2$	$Ga(NO_3)_3$	$Fe(NO_3)_3 \cdot 9H_2O$
$La_{0.5}Sr_{0.5}Ga_{0.2}Fe_{0.8}O_{3-\delta}$	4.330	2.116	1.023	6.646
$La_{0.6}Sr_{0.4}Ga_{0.2}Fe_{0.8}O_{3-\delta}$	5.196	1.693	1.023	6.646
$La_{0.6}Sr_{0.4}Ga_{0.3}Fe_{0.7}O_{3-\delta}$	5.196	1.693	1.534	5.656
$La_{0.6}Sr_{0.4}Ga_{0.4}Fe_{0.6}O_{3-\delta}$	5.196	1.693	2.046	4.848
$La_{0.7}Sr_{0.3}Ga_{0.2}Fe_{0.8}O_{3-\delta}$	6.062	1.270	1.023	6.646
$La_{0.7}Sr_{0.3}Ga_{0.3}Fe_{0.7}O_{3-\delta}$	6.062	1.270	1.534	5.656
$La_{0.7}Sr_{0.3}Ga_{0.4}Fe_{0.6}O_{3-\delta}$	6.062	1.270	2.046	4.848
$La_{0.7}Sr_{0.3}Ga_{0.5}Fe_{0.5}O_{3-\delta}$	6.062	1.270	2.557	4.04
$La_{0.7}Sr_{0.3}Ga_{0.6}Fe_{0.4}O_{3-\delta}$	6.062	1.270	3.067	3.232
$La_{0.7}Sr_{0.3}Ga_{0.7}Fe_{0.3}O_{3-\delta}$	6.062	1.270	3.580	2.424
$La_{0.8}Sr_{0.2}Ga_{0.2}Fe_{0.8}O_{3-\delta}$	6.928	0.847	1.023	6.646
$La_{0.8}Sr_{0.2}Ga_{0.3}Fe_{0.7}O_{3-\delta}$	6.928	0.847	1.534	5.656
$La_{0.8}Sr_{0.2}Ga_{0.4}Fe_{0.6}O_{3-\delta}$	6.928	0.847	2.046	4.848
$La_{0.8}Sr_{0.2}Ga_{0.5}Fe_{0.5}O_{3-\delta}$	6.928	0.847	2.557	4.04
$La_{0.8}Sr_{0.2}Ga_{0.6}Fe_{0.4}O_{3-\delta}$	6.928	0.847	3.067	3.232
$La_{0.8}Sr_{0.2}Ga_{0.7}Fe_{0.3}O_{3-\delta}$	6.928	0.847	3.580	2.424

4.3 Perovskite membrane preparation

Perovskite compounds were used to prepare perovskite membranes. The compounds were ground with acetone in mortar. Then the compounds were loaded into the cavity of KBr die that coated with wax and oil. The die having the perovskite compounds inside was knocked against table for 2-3 times to evaporate the air inside the compounds. The plunger was pressed to the surface of the compounds after assembled the die and then slowly applied the pressing pressure about 5 tons on the plunger of the die by the uniaxial pressing machine. The pressure was released and then the die was removed from the pressing machine after 10 minutes and then the green disc is around 1 mm thick, 13 mm diameter from 350-500 mg of compound were stripped from the die and plunger. Then the green disc was sintered in air at 1,200-1,350 ^{o}C for 10 hours. The sintering condition was as follows: the sample was heated to (1) 100 ^{o}C for 2 hours with the heating rate of 1.0 ^{o}C/min., (2) to 500 ^{o}C with the same heating rate and kept at 500 ^{o}C for 2 hrs, and (3) to 1,200-1,300 ^{o}C with the heating rate of 1.0 ^{o}C/min. Finally the sample was cooled to room temperature.

4.4 Characterization of the perovskite oxide

4.4.1 X-ray diffractometry (XRD)

The phase formations of perovskite compound and membrane were investigated by using X-Ray Diffractometer (D8 Avance, Bruker). Specimens were ground and pressed on slide before put in specimen slot of X-Ray Diffractometer. The experiment diffraction patterns were collected at room temperature over a range of 20-70° (step time 1s. and scan step 0.050^{o}).

The phase formations of perovskite compounds were characterized before and after calcination, and the phase transformation of membrane was also characterized by XRD.

4.4.2 Scanning electron microscopy (SEM)

The morphology of the compound and membrane discs was carried out using the SEM (ISM-6400) at the Scientific and Technological Research Equipment Center (STREC), Chulalongkorn University. This instrument uses X rays or electrons scattered back from the surface "illuminated" by a restored electron beam to generate an image with remarkable three-dimensional qualities. Specimens were sputter coated with gold to reduce charge effects.

CHAPTER 5

RESULTS AND DISCUSSION

The perovskites were prepared by the modified citrate method, each perovskite compound is indicated by the abbreviation using the initial letters of each metal in A and B sites sequentially, followed by the corresponding number which refers to the proportion of each metal in the compound. For example, $La_{0.6}Sr_{0.4}Ga_{0.2}Fe_{0.8}O_{3-\delta}$ and $La_{0.8}Sr_{0.2}Ga_{0.6}Fe_{0.4}O_{3-\delta}$ are abbreviated as LSGF 6428 and LSGF 8264, respectively.

5.1 Perovskite compound

5.1.1 Tolerance number of $La_{1-x}Sr_xGa_{1-y}Fe_yO_{3-\delta}$ perovskites

From the literature reviews [2, 6, 10, 11, 17, 18, 28, 36, 42, 43, 48], few works involved the synthesis of citrate method [17, 18] and modified citrate method [6]. Several of $La_{1-x}Sr_xGa_{1-y}Fe_yO_{3-\delta}$ perovskites, which have never been synthesized by modified citrate method, have thus been selected as revealed in tolerance number.

Generally the perovskites that have tolerance number higher 0.75 have a cubic structure indicating that they are possible to be single phase perovskite. The calculation for tolerance number is shown in Appendix A. In the previous study, it was found that the synthesized perovskite by modified citrate method will be the single phase when Sr/Fe less than 0.63.

Accordingly, all the compounds in Table 5.1 are possibly the single phase perovskite.

Table 5.1 Tolerance number of the synthesized perovskites

Number	Compounds	Tolerance No.
1	LSGF 5528	1.00
2	LSGF 6428	1.10
3	LSGF 6437	1.10
4	LSGF 6446	1.10
5	LSGF 7328	1.20
6	LSGF 7337	1.20
7	LSGF 7346	1.20
8	LSGF 7355	1.19
9	LSGF 7364	1.19
10	LSGF 7373	1.19
11	LSGF 8228	1.31
12	LSGF 8237	1.30
13	LSGF 8246	1.30
14	LSGF 8255	1.29
15	LSGF 8264	1.29
16	LSGF 8273	1.29

5.1.2 Synthesis of perovskite compound by modified citrate method

By modified citrate method, the metal nitrates are dissolved in 70% nitric acid, which then react with citric acid to form metal-citrate-nitrate complexes. These metal-citrate complexes can undergo polymerization when ammonium hydroxide (NH_4OH) is added. When NH_4OH was added, the white fume of NH_4NO_3 suddenly appeared, which came from the free NO_3^- reacting with NH_4OH and generating heat. In the case of LSGF 6428, the colour of the mixture had been changed from dark brown (pH<1) to clear brown and fume generation stopped at pH$\approx$1. At this point, the remained citric acid and NH_4NO_3 might dissolve in the solution due to the added NH_4OH (10 ml). Then the solution was changed to clear yellow solution (pH$\approx$1.5) and to yellow precipitation (pH$\approx$3-6). This precipitation indicated the metal-citrate-

nitrate gel resulting from the polymerization of the metal-citrate-nitrate complex when NH$_4$OH was increased [17]. Then the solution is changed to clear brown solution (pH≈ 9).

The combustion of the metal-citrate-nitrate gel solution was composed of three steps; evaporation, decomposition, and spontaneous combustion. The excess solvent was firstly evaporated until a sticky gel was obtained. During the final stage of evaporation, the mixture began to swell, and became viscous. The generated gases were evolved from the large swelling viscous mass. Finally, at around 200°C the spontaneous combustion was initiated and the mixture was transformed into the compound. A typical burning of 40 ml of gel solution was completed within 10-20 seconds.

The equation for the formation of these perovskites assuming complete combustion of the redox mixtures containing citric acid, for example, LSGF, can be written as in Equation (5.1).

$(1-x)La(NO_3)_3 + xSr(NO_3)_2 + (1-y)Ga(NO_3)_3 + yFe(NO_3)_3 + 2HOC(COOH)(CH_2COOH)_2$

$$\downarrow$$

$$La_{1-x}Sr_x Ga_{1-y}Fe_yO_{3-\delta} \text{ (s)} + 12CO_2 \text{ (g)} + 8H_2O \text{ (g)} + 3N_2 \text{ (g)} \qquad (5.1)$$
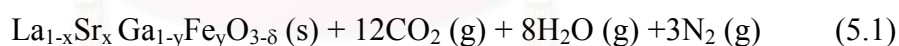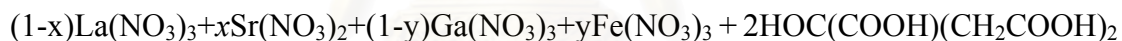
Two moles of citric acid are required to react with 2 moles of all combined metal nitrates. In other words, the total metals will react with citric acid in the approximately equimolar ratio. However, in practice, the excess amount of citric acid was used to assure the complete reaction of all the metal nitrates. Normally, three moles of citric acid was used to react with 2 moles of the total metal nitrates. Therefore, every three molecules of citric acid originally present, one remained uncombined and was removed from the mixture later by either evaporation or decomposition to yield carbon dioxide and water during heating in the vacuum oven. However, the citric acid twice as much as the total metal nitrate was used in the synthesis of each perovskites in this research.

The postulated mechanism of perovskite formation has already been proposed by Yeyongchaiwat [56]. This mechanism is presented in Scheme 5.1.

$$(1\text{-}x)La(NO_3)_3 + xSr(NO_3)_2 + (1\text{-}y)Ga(NO_3)_3 + yFe(NO_3)_3 + 2HOC(COOH)(CH_2COOH)_2$$

$\downarrow$ **70% HNO$_3$**

Metal-citrate complexes

$\downarrow$ **NH$_4$OH**

Metal citrate-nitrate gel

$\downarrow$ **Heat**

$$La_{1-x}Sr_x Ga_{1-y}Fe_yO_{3-\delta} \text{ (s)} + 12CO_2 \text{ (g)} + 8H_2O \text{ (g)} + 3N_2 \text{ (g)}$$
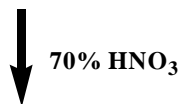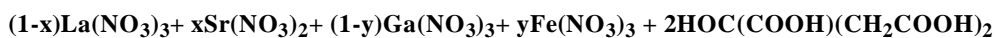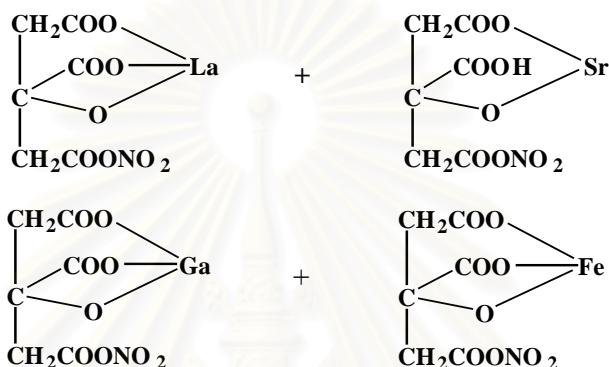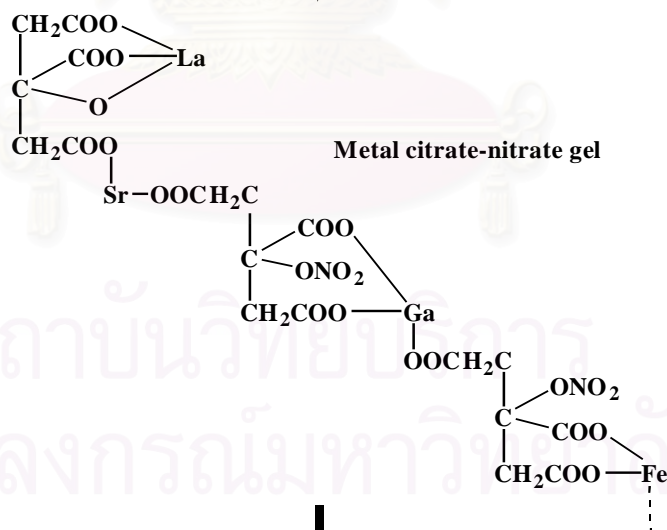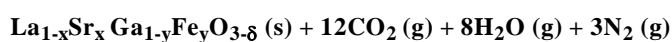
Scheme 5.1 The postulated mechanism of the perovskite formation

The experimental conditions and data for the synthesis of all perovskite compounds are shown in Table 5.2.

Table 5.2 List of the experimental conditions for synthesis of the perovskite compounds

Compounds	Solution colour		Colour of solution and appearance changing during titration	pH	Material feature
	Nitric acid	Citric acid			
LSGF 5528	Yellow	Dark brown	Dark brown to yellow to precipitate to clear brown	9.13	Fluffy black and black compound
LSGF 6428	Yellow	Dark brown	Dark brown to yellow to precipitate to clear brown	8.88	Fluffy yellow and gray compound
LSGF 6437	Yellow	Dark brown	Dark brown to yellow to precipitate to clear brown	9.04	Fluffy yellow and gray compound
LSGF 6446	Yellow	Dark brown	Dark brown to yellow to precipitate to clear brown	8.94	Fluffy yellow and gray compound
LSGF 7328	Yellow	Dark brown	Dark brown to yellow to precipitate to clear brown	8.70	Fluffy yellow and gray compound
LSGF 7337	Yellow	Dark brown	Dark brown to yellow to precipitate to clear brown	9.06	Fluffy yellow and gray compound
LSGF 7346	Yellow	Dark brown	Dark brown to yellow to precipitate to clear brown	9.05	Fluffy yellow and gray compound
LSGF 7355	Yellow	Dark brown	Dark brown to yellow to precipitate to clear brown	9.03	Fluffy yellow and gray compound
LSGF 7364	Yellow	Dark brown	Dark brown to yellow to precipitate to clear brown	9.13	Fluffy yellow and gray compound
LSGF 7373	Yellow	Dark brown	Dark brown to yellow to precipitate to clear brown	9.07	Fluffy yellow and gray compound
LSGF 8228	Yellow	Dark brown	Dark brown to yellow to precipitate to clear brown	8.98	Fluffy yellow and gray compound
LSGF 8237	Yellow	Dark brown	Dark brown to yellow to precipitate to clear brown	9.09	Fluffy yellow and gray compound

Table 5.2 List of the experimental conditions for synthesis of the perovskite compounds (continued)

Compounds	Solution colour		Colour of solution and appearance changing during titration	pH	Material feature
	Nitric acid	Citric acid			
LSGF 8246	Yellow	Dark brown	Dark brown to yellow to precipitate to clear brown	9.15	Fluffy yellow and gray compound
LSGF 8255	Yellow	Dark brown	Dark brown to yellow to precipitate to clear brown	8.91	Fluffy yellow and gray compound
LSGF 8264	Yellow	Dark brown	Dark brown to yellow to precipitate to clear brown	8.89	Fluffy yellow and gray compound
LSGF 8273	Yellow	Dark brown	Dark brown to yellow to precipitate to clear brown	8.97	Fluffy yellow and gray compound

5.1.3 Characterization of the phase of perovskite compound after calcinations at 800°C

All $La_{1-x}Sr_xGa_{1-y}Fe_yO_{3-\delta}$ perovskite compounds in Table 5.1 were calcined at 800°C to eliminate the carbon residue. Then the phase formation of each compound was characterized by XRD technique.

In the XRD analysis, the shape and size of the unit cell can be calculated from the angular positions of the diffraction lines (peaks), and the arrangement of the atoms within the unit cell can be calculated from the relative intensities of the lines. If the single phase perovskite with a cubic structure is formed the diffraction lines at the reflective planes 100, 110, 111, 200, 210, 211, and 220 must be observed [57]. In case of LSGF 8228, all these diffraction lines appear as shown in Figure 5.1. Therefore, LSGF 8228 is the single phase perovskite. The appearance of the splitting peaks indicates the distortion from the cubic structure and the presence of the diffraction lines other than those will be due to the other compound or secondary phase.
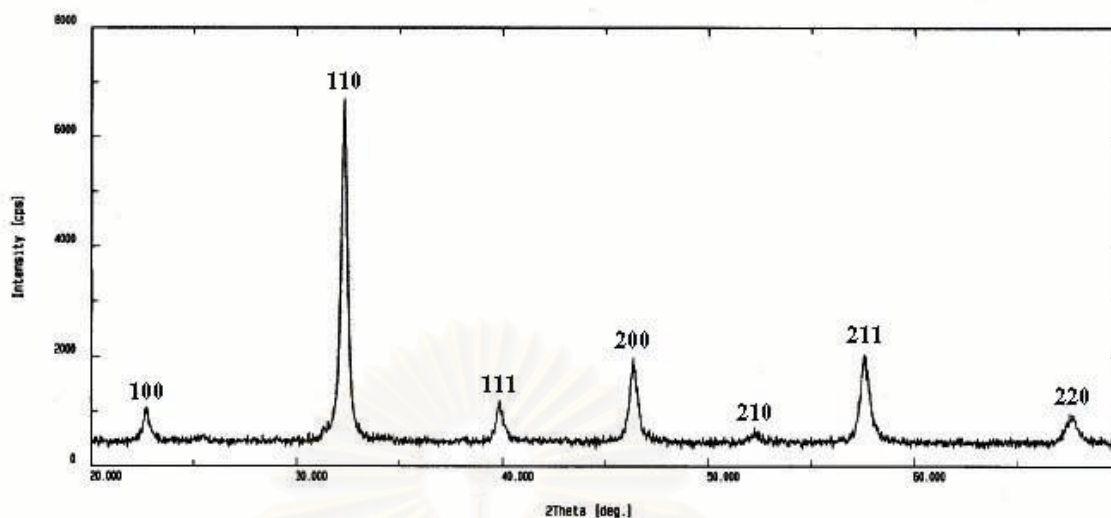
Figure 5.1 Diffraction lines at the reflective planes of the single phase perovskite type LSGF 8228 with a cubic structure.

5.1.3.1 La$_{0.5}$Sr$_{0.5}$Ga$_{1-y}$Fe$_y$O$_{3-\delta}$ perovskite compound

Figure 5.2 shows the XRD pattern of LSGF 5528, which is the only compound in this series.

The diffraction lines of 2 theta = 22.5, 32.0, 40.0, 47.0, 52.5 and 58.0 (marked with ●) belong to LaSrGaFeO$_3$. Another set of the diffraction lines, marked with ▼, may be the other oxide compounds such as Ga$_2$O, La$_2$O, SrO, SrGaO$_7$, SrLaGaO$_4$ and La$_4$SrO$_7$. By comparing with the XRD patterns of the standard compound, it could be identified as SrLaGaO$_4$ (JCPDS-database: 24-1208) [56]. In other words, SrLaGaO$_4$ exists as the secondary phase. It clearly exhibits the mixture of LaSrGaFeO$_3$ and SrLaGaO$_4$ as major and minor compounds, respectively. Accordingly, this compound is not a single phase after calcined at 800°C.
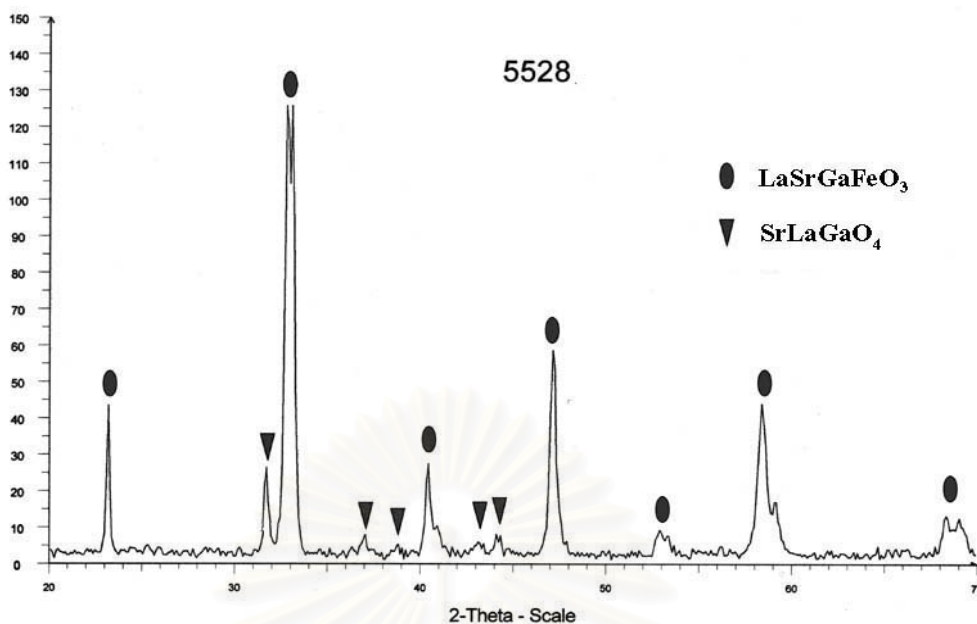
Figure 5.2 XRD pattern of LSGF 5528 perovskite after calcined at 800°C.

5.1.3.2 $La_{0.6}Sr_{0.4}Ga_{1-y}Fe_yO_{3-\delta}$ perovskite compounds

In this series, LSGF 6428, LSGF 6437 and LSGF 6446 were synthesized. From Figure 5.3, an XRD pattern of LSGF 6428 shows the diffraction lines, which belong to the $LaSrGaFeO_3$ set. This concludes that LSGF 6428 is the single phase perovskite. In case of LSGF 6437, other small diffraction lines are observed indicating that the existence of the secondary phase of $SrLaGaO_4$ but LSGF 6446 is not shown that the secondary phase was clearly observed.
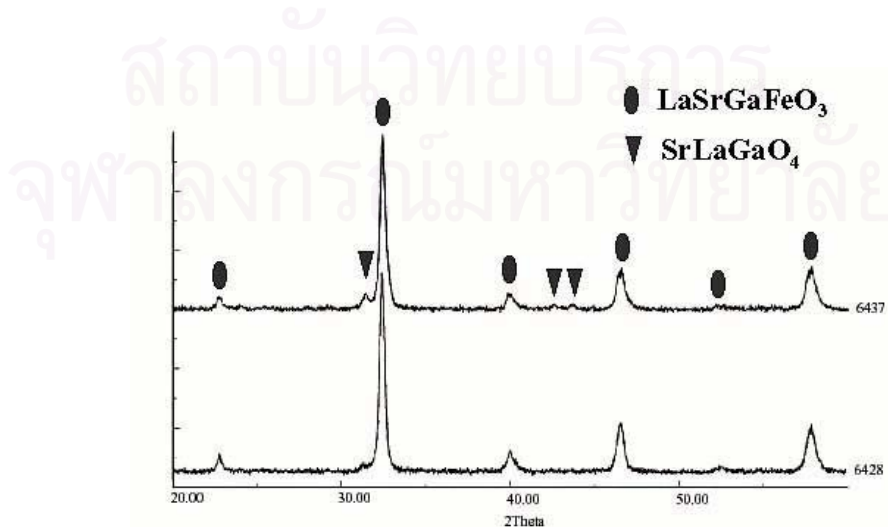
Figure 5.3 LSGF 6428 and LSGF 6437 perovskites after calcined at 800°C.

5.1.3.3 La$_{0.7}$Sr$_{0.3}$Ga$_{1-y}$Fe$_y$O$_{3-\delta}$ perovskite compounds

Figure 5.4 illustrates the XRD patterns of LSGF 7328, LSGF 7337, LSGF 7346, LSGF 7355, and LSGF 7364 but not includes LSGF 7373.

All these compounds contain LaSrGaFeO$_3$ but the existence of SrLaGaO$_4$ as the secondary phase was observed for LSGF 7337, LSGF 7346, LSGF 7355, LSGF 7364 and LSGF 7373. It should be noted that LaSrGaFeO$_3$ and SrLaGaO$_4$ decreases and increases, respectively, with higher Ga content in the compound. Therefore, only LSGF 7328 is the single phase perovskite.
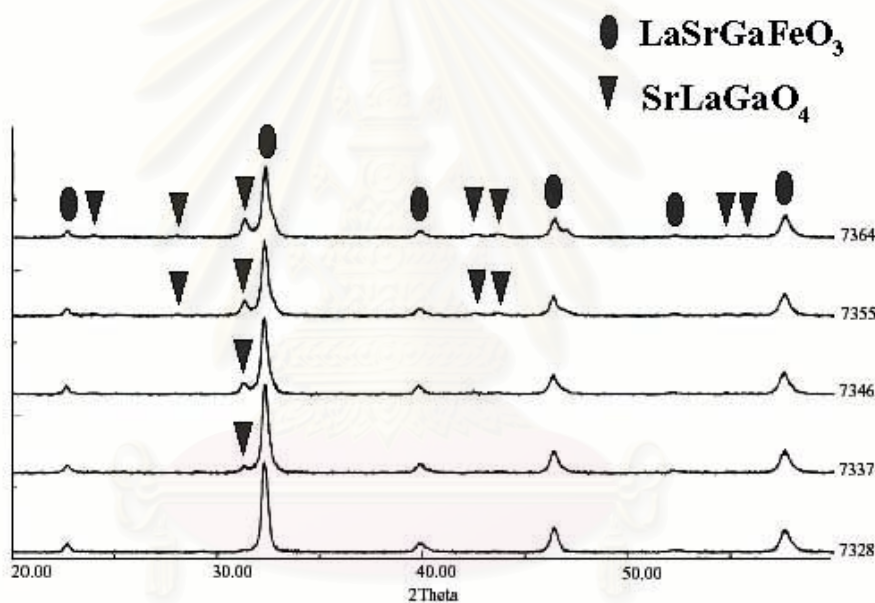
Figure 5.4 XRD patterns of LSGF 7328, LSGF 7337, LSGF 7346, LSGF 7355 and LSGF 7364 perovskites after calcined at 800°C.

5.1.3.4 La$_{0.8}$Sr$_{0.2}$Ga$_{1-y}$Fe$_y$O$_{3-\delta}$ perovskite compounds

In the similar pattern, the single phase of LSGF 8228 and LSGF 8237 obtained are shown in Figure 5.5. The secondary phase SrLaGaO$_4$ of compound slightly increased with increasing Ga content and decreasing Fe content.

All these compounds contain LaSrGaFeO$_3$ but the existence of SrLaGaO$_4$ as the secondary phase is observed for LSGF 8246, LSGF 8255 and LSGF 8264, and LSGF 8273 that not included in Figure 5.5. It should be noted that LaSrGaFeO$_3$ and SrLaGaO$_4$ decreases and increases, respectively, with higher Ga content in the compound. Consequently, LSGF 8228 and LSGF 8237 are the single phase perovskite.
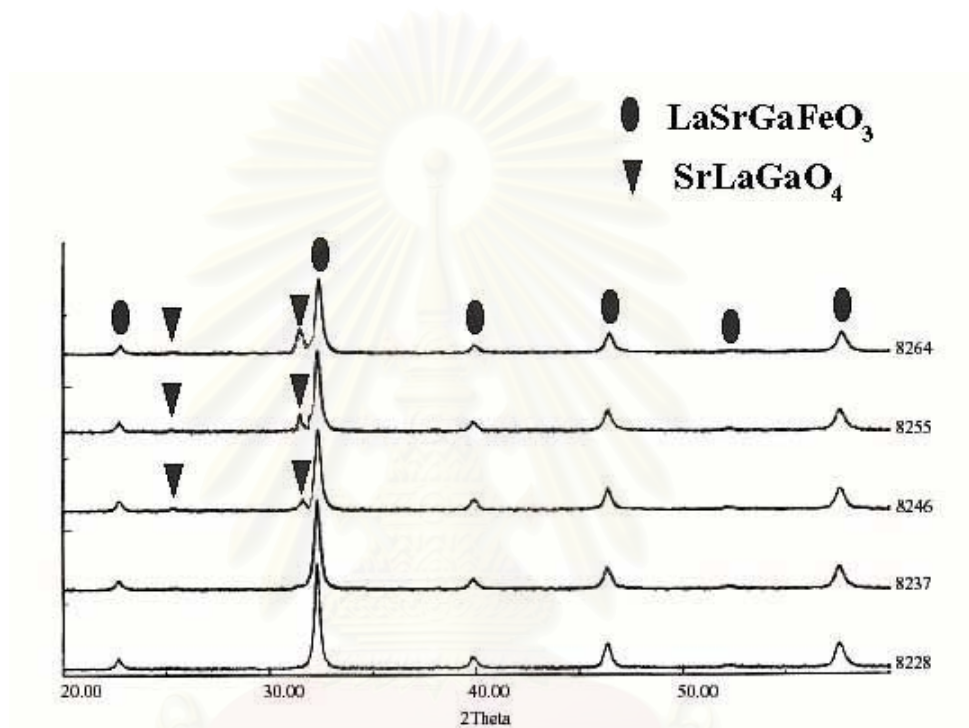
Figure 5.5 XRD patterns of LSGF 8228, LSGF 8237, LSGF 8246, LSGF 8255 and LSGF 8264 perovskites after calcined at 800°C.

5.1.4 Effect of composition on the formation of LaGaO$_3$-based perovskite

In the previous section, it can be concluded that four of sixteen compounds are the single phase perovskite. The rest compounds can be classified into two groups, referring to the secondary phase content by the intensity ratio of the diffraction line at $2\theta = 32.5$ and 32 of LaSrGaFeO$_3$ and SrLaGaO$_4$, respectively. The ratio is lower than 9.26 as defined to the clearly observed secondary phase and the ratio 9.26-11.50 is due to the trace amount of secondary phase as shows in Table 5.3.

Table 5.3 Classification of the synthesized perovskite compounds.

Compounds	Intensity ratio*	Phase observing
LSGF 6428	-	Single phase
LSGF 7328	-	Single phase
LSGF 8228	-	Single phase
LSGF 8237	-	Single phase
LSGF 6437	11.50	Trace of secondary phase
LSGF 7337	10.10	Trace of secondary phase
LSGF 8246	9.54	Trace of secondary phase
LSGF 7346	9.26	Trace of secondary phase
LSGF 5528	6.12	Secondary phase
LSGF 7355	5.64	Secondary phase
LSGF 8255	5.33	Secondary phase
LSGF 7364	4.44	Secondary phase
LSGF 8264	4.20	Secondary phase
LSGF 6446	Not available	Secondary phase
LSGF 7373	Not available	Secondary phase
LSGF 8273	Not available	Secondary phase

* The intensity ratio of the diffraction line at $2\theta = 32.5$ and 32 of $LaSrGaFeO_3$ and $SrLaGaO_4$, respectively.

The existence of the secondary phase in some perovskite compounds can be derived from the amount of Sr and Fe incorporated in the structure. Therefore, the variation of Sr and Fe contents on the perovskite formation is discussed in this section.

5.1.4.1 The effect of Sr content on the phase formation

To illustrate the effect of Sr content on the phase formation, the perovskite compounds with the same Fe content will be grouped together. Therefore, four groups of the perovskite compounds are shown in Table 5.4.

When the composition of Fe is 0.8 such as LSGF 5528, LSGF 6428, LSGF 7328 and LSGF 8228, the secondary phase was observed only in LSGF 5528 and the others were the single phase. This means that the Sr content should be less than 0.5 when Fe = 0.8. For the composition of Fe = 0.7, LSGF 6437, LSGF 7337, and LSGF 8237 shows the same trend in Fe content = 0.8 that the secondary phase slightly increased with the increasing of Sr content. The similar phenomenon was reported by Mori et al. [53] that the higher Sr content in lanthanum chromites caused the appearance of higher amounts of secondary phase.

It suggests that excessive of Sr content affects the phase formation. The explanation is that the partial substitution of La (1.36 ^{o}A) with the bigger ion, Sr (1.44^{o}A) in the LaGaO$_3$ lattice, is not completed leading to the formation of SrLaGaO$_4$, the secondary phase.

When the Fe content decreases to 0.6 or lower and Sr content is 0.2 and 0.3; namely LSGF 7346, LSGF 7355, LSGF 8246 and LSGF 8255, the secondary phase appeared in all of them. This suggested that the single phase formation of LSGF depends on Fe content that will be discussed in next section.

Table 5.4 Secondary phases found in various Sr-doped LSGFs

Compounds	Observed secondary phases
LSGF 5528	Yes
LSGF 6428	No
LSGF 7328	No
LSGF 8228	No
LSGF 6437	Traces
LSGF 7337	Traces
LSGF 8237	No
LSGF 7346	Yes
LSGF 8246	Yes
LSGF 7355	Yes
LSGF 8255	Yes

5.1.4.2 The effect of Fe content on the phase formation

The effect of Fe content on the phase formation, the perovskite compounds with the same Sr content is classified into three groups that illustrated in Table 5.5.

The composition of Sr = 0.2 in LSGF 8228, LSGF 8237, LSGF 8246, LSGF 8255 and LSGF 8264, it was found that the secondary phase gradually increased. In the composition of Sr = 0.3, LSGF 7328, LSGF 7337, LSGF 7346, LSGF 7355 and LSGF 7364, and the composition of Sr = 0.4, LSGF 6428 and LSGF 6437 showed the similar results, the amount of secondary phase trended to form with the decreasing of Fe or the increasing of Ga. This result was also supported by Yeyongchaiwat's research [56].

Considering the concentration of Fe and Ga in all composition, the concentration of Fe is more than that of Ga and the structure of $LaFeO_3$ is more stable than $LaGaO_3$ [48]. Therefore the mainframe of perovskite structure is $LaFeO_3$ and Ga is a dopant. When the excessive amount of Ga was added, $SrLaGaO_4$ or secondary phase is formed that can be explained by the ion size of Ga and Fe that Ga (0.62^{o}A)

larger than Fe (0.55^{o}A). It can be concluded that the secondary phase increased with the increasing of Ga content or the decreasing of Fe content.

Table 5.5 Secondary phases found in various Fe-doped LSGF

Compounds	Observed secondary phases
LSGF 6428	No
LSGF 6437	Traces
LSGF 7328	No
LSGF 7337	Traces
LSGF 7346	Traces
LSGF 7355	Yes
LSGF 7364	Yes
LSGF 8228	No
LSGF 8237	No
LSGF 8246	Traces
LSGF 8255	Yes
LSGF 8264	Yes

5.2 Perovskite membrane

The single phase perovskite, LSGF 6428, LSGF 7328, LSGF 8228 and LSGF 8237, and the single phase with traces of secondary phase perovskite compounds, LSGF 6437, LSGF 7337, LSGF 7346, and LSGF 8246 were selected to prepare the membrane.

It has been supported by Yeyongchaiwat [56] that PVA and PEG 400 were used as binders for membrane perovskite but very large pores were developed in the resulted membrane after sintering. In addition, the membrane perovskite without binder using pressing pressure 5 tons was primarily attempted in this study, it was found that the membrane was obtained. Therefore, the binder was not used in this research.

The effect of pressing pressure, sintering time and composition on the morphology had been investigated. In addition, the sintering temperature on the phase transformation and the density of perovskite membrane were studied.

5.2.1 The perovskite membrane morphology

5.2.1.1 Effect of pressing pressure

The effect of pressing pressure on the green discs was studied by considering the morphology of membranes with the variation of pressing pressure. In this experiment, LSGF 7328 compound was selected for preparing the membrane using pressing pressure 5 tons and 7 tons. It was then sintered at 1,250^{o}C for 10 hours. Figure 5.6 shows SEM micrographs of the perovskite membrane. They have very similar features even though the slightly smaller void or pore size can be observed in case of the membrane prepared by using pressing pressure 7 tons. Due to insignificant difference, it was chosen to press with pressure 5 tons in order to avoid the membrane breaking problem.
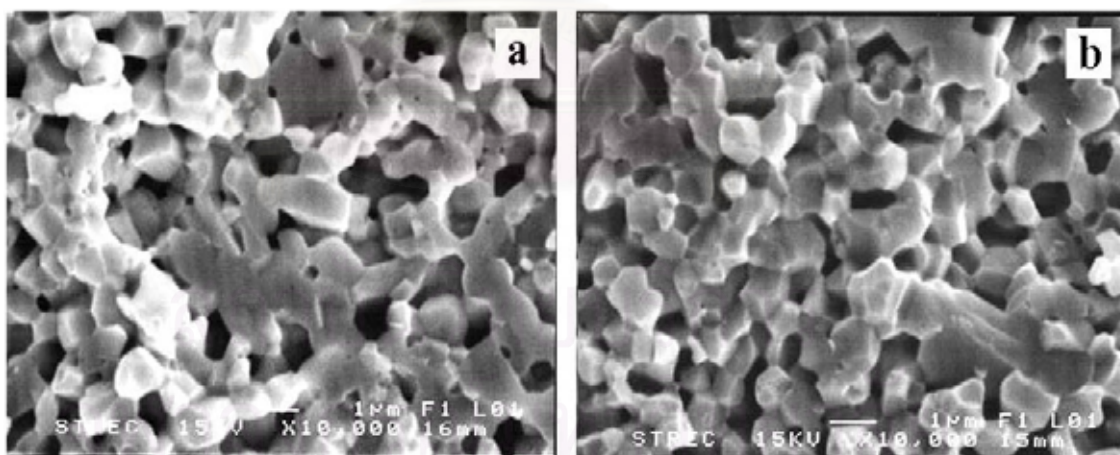
Figure 5.6 SEM pictures of cross section of LSGF 7328 samples sintered at 1,250^{o}C for 10 hours with pressure pressing 5 tons (a) and 7 tons (b)

5.2.1.2 Effect of sintering time

LSGF 7328 membrane was prepared by using pressure 5 tons and then sintering at 1,200^{o}C for different period of time, 10 hours and 15 hours. Figure 5.7 exhibits very similar feature of both membrane. This indicates that it is not necessary to sinter the membrane longer than 10 hours. Therefore, the sintering time for 10 hours was applied in the following experiments.
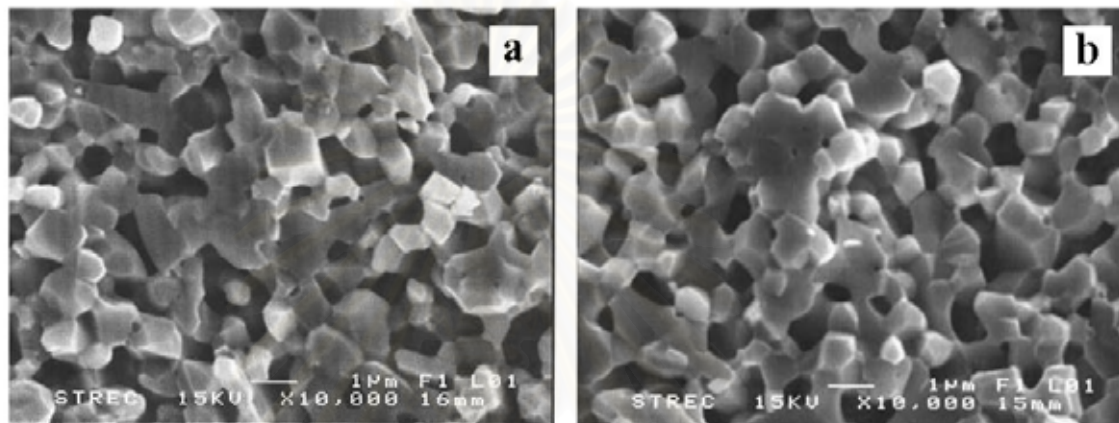
Figure 5.7 SEM pictures of cross section of LSGF 7328 samples sintered at 1,250^{o}C for 10 hours (a) and 15 hours (b)

5.2.1.3 Effect of chemical composition on the morphology of perovskite membrane

In this section, the morphology of perovskite membrane, with various Sr and Fe contents was investigated by SEM technique.

5.2.1.3.1 Effect of Sr content

In this experiment, LSGF 8228, LSGF 7328 and LSGF 6428 membrane were selected for comparison. These three perovskites had equal proportion of Ga and Fe and all of them in powder form had already been identified as the single phase perovskites. The membrane of each one was made by using pressing pressure 5 tons. They were then sintered at 1,250^{o}C for 10 hours. Figure 5.8 exhibits the SEM in cross section pictures of LSGF 8228, LSGF 7328 and LSGF 6428 perovskite

membranes after sintering. It can be seen that LSGF 6428 had larger grain size than LSGF 7328 and LSGF 8228 respectively. It is obvious that the difference in grain size must result from amount of Sr in each perovskite. It should indicate that the doped Sr in $LaGaO_3$ decreased the melting point but the dependence of Sr doping on the melting point is not clear [58]. This means that at the same sintering temperature, the density of membrane would be increased with the amount of Sr. The similar phenomenon was reported by Mori et al. [53]. They synthesized the $La_{1-x}Sr_xCrO_3$ membranes, which the compound was synthesized by solid state method. The membrane was sintered at $1,600^oC$ for 10 hours. The results also showed that the density increased with increasing Sr content. It indicated that the Sr content is indispensable in obtaining dense perovskite membrane.

Therefore the grain size of LSGF 6428 was larger than LSGF 7328 and LSGF 8228, respectively.
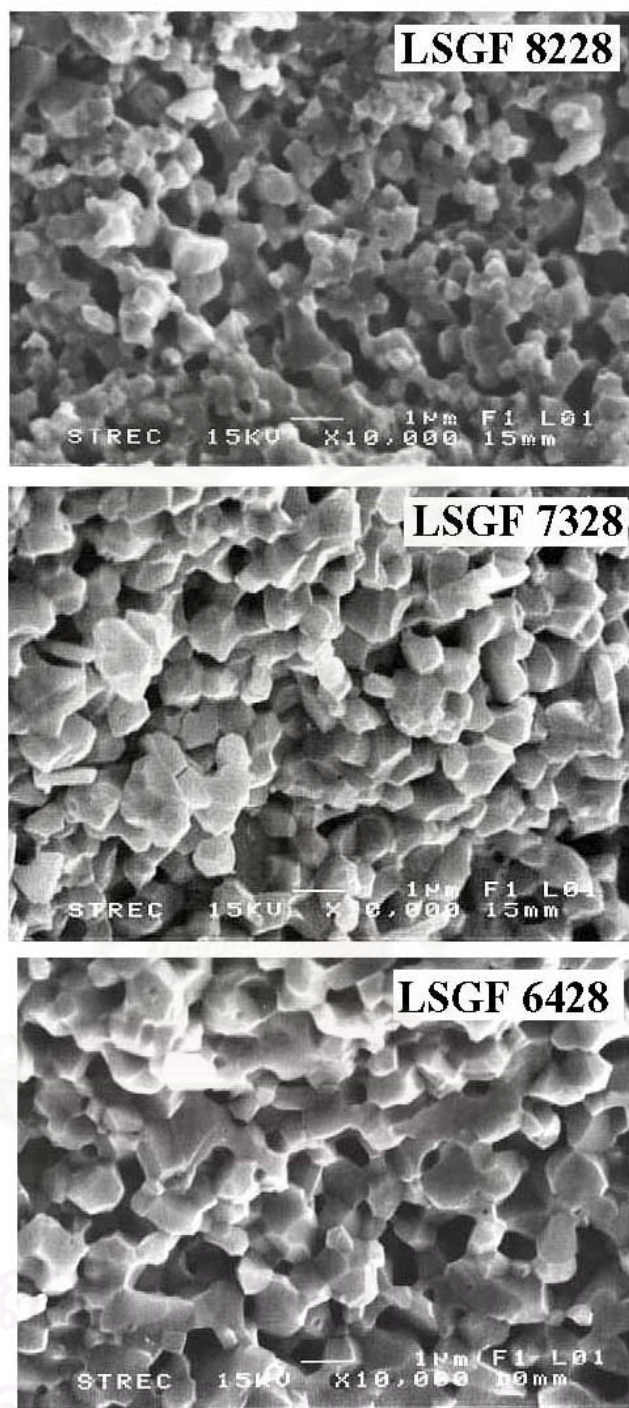
Figure 5.8 SEM pictures of cross section of LSGF 8228, LSGF 7328 and

LSGF 6428 membranes sintered at 1,250$^{\text{o}}$C for 10 hours.

5.2.1.3.2 Effect of Fe content

The morphology of membranes was investigated when Fe content is varied. LSGF 7328 and LSGF 7337 membrane after sintering at $1,200^{o}C$ for 10 hours, and LSGF 8228 and LSGF 8246 after sintering at $1,300^{o}C$ for 10 hours were selected as displayed in Figure 5.9. The melting and the density of perovskites improved with the decreasing of Fe. It is shown that the morphology of the membrane depends on the concentration of Fe that explained by the stability of structure on the sintering temperature, $LaFeO_3$ was more stable than $LaGaO_3$ [48]. Therefore the higher Fe content, LSGF 7328 and LSGF 8228 have the stability more than the lower Fe content, LSGF 7337 and LSGF 8246, respectively. The welding of LSGF 7328 and LSGF 8228 is also lower than LSGF 7337 and LSGF 8246, respectively.

This result is contrast with the previous research of Yeyongchaiwat [56]. She reported that the grain size diameter around 1 m was observed in all $La_{0.6}Sr_{0.4}Ga_{1-y}Fe_yO_{3-}$ membranes. Therefore, she concluded that the grain growth phenomenon was not found when the Fe content increased. This result can be explained that because $La_{0.6}Sr_{0.4}Ga_{1-y}Fe_yO_{3-}$ membranes have the large grain size. Therefore, it cannot clearly observe the differentia of grain size but in LSGF 7328 and LSGF 8246 membrane, this phenomenon was clearly observed because of the smaller grain size.

It indicated that the density of perovskite membrane depended on the decreasing of Fe or the increasing of Ga content. At the same sintering temperature, the welding and density in LSGF 7337 and LSGF 8246 are larger than LSGF 7328 LSGF 8228, respectively.
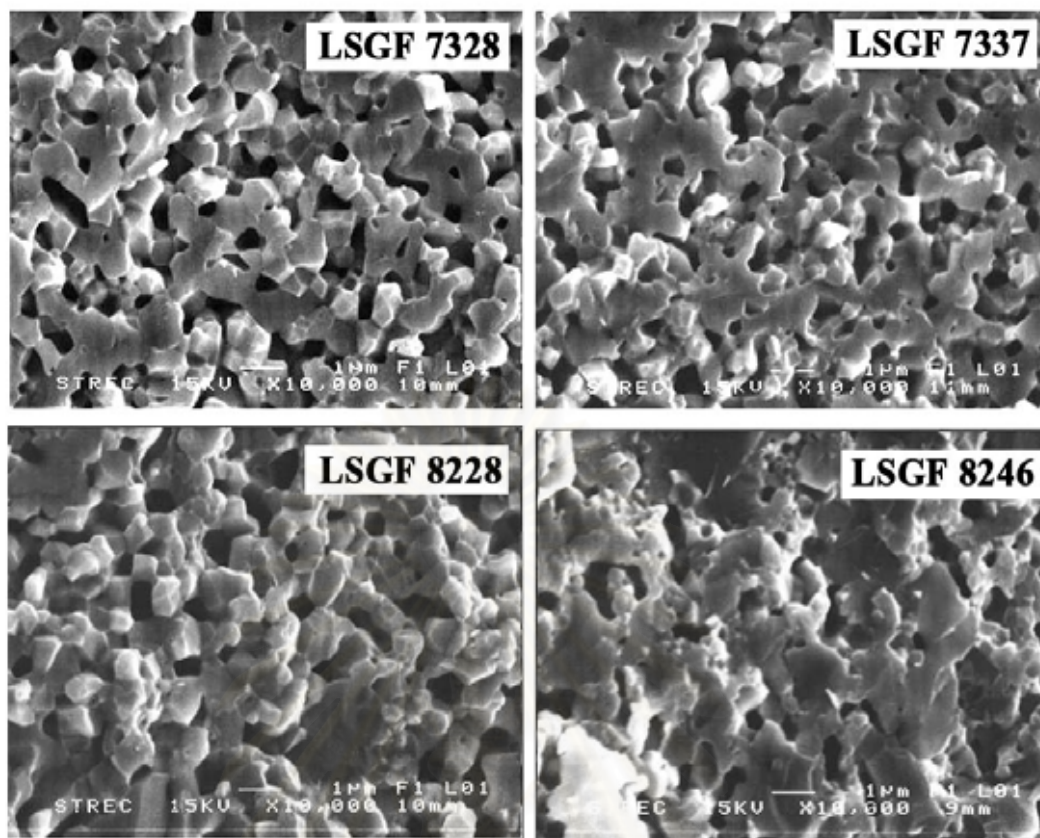
Figure 5.9 SEM pictures of cross section of LSGF 7328 and LSGF 7337 membranes sintered at 1,200°C for 10 hours, and LSGF 8228 and LSGF 8246 sintered at 1,300°C for 10 hours

5.2.2 Effect of sintering temperature on the phase transformation of perovskite membrane

The single phase perovskite, LSGF 6428, LSGF 7328, LSGF 8228 and LSGF 8237, and the single phase with traces of secondary phase perovskite compounds, LSGF 6437, LSGF 7337, LSGF 7346, and LSGF 8246 were selected to prepare the membrane and sintered at 1,200 - 1,350°C. The effect of sintering temperature on the phase transformation of these membranes was investigated. Figure 5.10 shows the XRD patterns of LSGF 7337 membrane at various sintering temperatures (1,200 - 1,350°C). It is shown that LSGF 7337 at 1,200°C is the single phase and XRD pattern of LSGF 7337 at 1,250°C is the single phase with traces of secondary phase. At 1,300 - 1,350°C the secondary phase was clearly found. XRD analysis of these samples

reveals that the main phase is $LaSrGaFeO_3$ in all temperatures. When the sintering temperature was increased amounts of secondary phase increased. It can be explained that the lattice of $LaSrGaFeO_3$ trended to decompose at high temperature, causing the formation of $LaSrGaO_4$ or secondary phases.

This phenomenon is corresponding with report of Ming et al. [48]. They revealed that the XRD patterns of $La_{0.5}Sr_{0.5}Ga_{0.2}Fe_{0.8}O_{3-\delta}$, which was synthesized by solid state method, showed the perovskite oxide remained cubic over the temperature range of 20 to $800^{\circ}C$. At $1,000^{\circ}C$, $La_{0.5}Sr_{0.5}Ga_{0.2}Fe_{0.8}O_{3-\delta}$ underwent decomposition, associated with the disappearance of the strongest peak of secondary phase. The XRD patterns between 800 and $900^{\circ}C$ indicated the decomposition of $La_{0.5}Sr_{0.5}Ga_{0.2}Fe_{0.8}O_{3-\delta}$ occurred at $860^{\circ}C$. It is confirmed that the secondary phase increased with the increasing of sintering temperature.
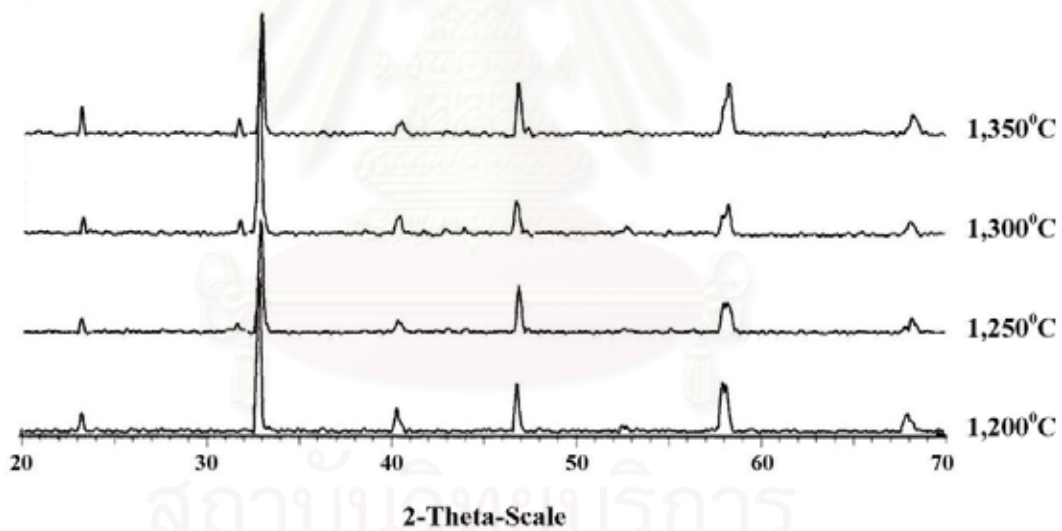
Figure 5.10 XRD patterns of LSGF 7337 perovskite membrane after sintered at 1,200- 1350°C

Table 5.6 listed the appearance of secondary phase for various types of LSGF membrane after sintering at 1,200 - 1,350°C.

The membranes prepared from the single phase perovskite compounds, LSGF 6428, LSGF 7328 and LSGF 8228, showed that the secondary phase slightly increased with increasing of sintering temperature. It is due to the effect of decomposition of LSGF lattice at high temperature. In perovskite type LSGF 8237, the secondary phase was found in XRD patterns of membrane at all sintering temperatures. As compared to the other membrane, LSGF 8237 has high tolerance number and less Fe content. Therefore its stability is less than LSGF 6428, LSGF 7328 and LSGF 8228.

In the XRD patterns of membranes prepared from the perovskite, which have single phase with traces of secondary phase such as LSGF 6437, LSGF 7337, LSGF 7346 and LSGF 8246, the similar trend was observed at sintering temperature 1,200-1,350^{o}C except LSGF 6437 and LSGF 7337 at 1,200^{o}C. For the membranes type LSGF 6437 and LSGF 7337, the traces of secondary phase disappeared after sintering at 1,200^{o}C. It might be due to the melting of secondary phase into the single phase.

For LSGF 7346 and LSGF 8246 after sintering at temperature 1,200-1,350^{o}C the secondary phase appeared because of the high tolerance number.

Table 5.6 Existence of secondary phases of LSGF membrane at various
sintering temperatures.

Types	Existence of secondary phase before sintering	Sintering temperature (^{o}C)	Existence of secondary phase
6428	No	1200	No
		1250	No
		1300	Traces
		1350	Traces
7328	No	1200	No
		1250	No
		1300	Traces
		1350	Traces
8228	No	1200	No
		1250	Traces
		1300	Traces
		1350	Traces
8237	No	1200	Yes
		1250	Yes
		1300	Yes
		1350	Yes
6437	Traces	1200	No
		1250	Yes
		1300	Yes
		1350	Yes
7337	Traces	1200	No
		1250	Traces
		1300	Traces
		1350	Yes
7346	Traces	1200	Yes
		1250	Yes
		1300	Yes
		1350	Yes
8246	Traces	1200	Yes
		1250	Yes
		1300	Yes
		1350	Yes

5.2.3 Effect of sintering temperature on the density of perovskite membrane

The single phase membranes, LSGF 7328 and LSGF 8228 were selected for this study. They were sintered at various temperatures, 1,200-1,350°C. When the sintering temperature was higher, the larger grain size was obtained in both cases. These results were certainly affected by high sintering temperature. At higher temperature, the welding of perovskite grains occurred. It indicated that sintering temperature is also indispensable in obtaining dense perovskite membrane.
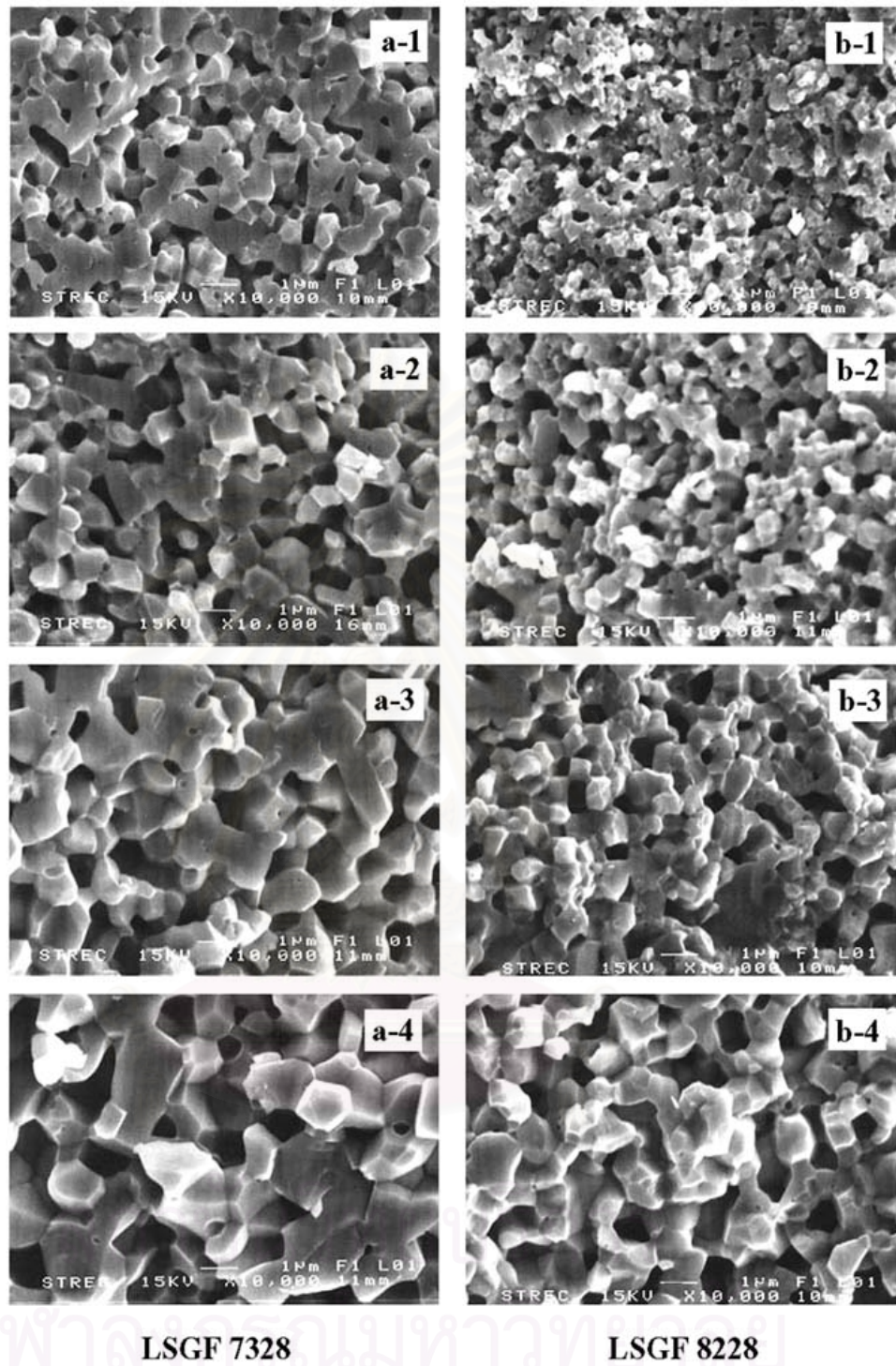
LSGF 7328　　　　**LSGF 8228**

Figure 5.11 SEM pictures of cross section of LSGF 7328 and LSGF 8228

samples sintered at 1,200 -1350°C for 10 hours.

(a-1) LSGF 7328 at 1,200 ^{o}C; (b-1) LSGF 8228 at 1,200 ^{o}C

(a-2) LSGF 7328 at 1,250 ^{o}C; (b-2) LSGF 8228 at 1,250 ^{o}C

(a-3) LSGF 7328 at 1,300 ^{o}C; (b-3) LSGF 8228 at 1,300 ^{o}C

(a-4) LSGF 7328 at 1,350 ^{o}C; (b-4) LSGF 8228 at 1,350 ^{o}C

The bulk density of perovskite membranes after sintering was determined by calculation from weight and volume of perovskite membrane after sintering (Appendix A). In case of LSGF 6428 and LSGF 7328, the bulk density of membrane was increased with the increasing sintering temperature as revealed in Table 5.7. This is due to the loss of mass of some oxide compounds, possibly Ga_2O_3 and Ga_2O vaporization during sintering [59, 60]. Furthermore, the grain welding also occurred as obviously seen by SEM as shown in Figure 5.11. This phenomenon caused the reduction of the membrane volume. However, at 1,300-1350 ^{o}C the bulk density decreased. This may be the effect of the formation of the secondary phase that derived form Ga_2O_3 and Ga_2O. This is consistent with the appearance of the diffraction lines of secondary phase in XRD (Appendix B).

The same explanation can be applied for LSGF 6437, LSGF 7337 and LSGF 8228. This is the bulk density decrease with the increasing sintering temperature from 1,250-1350 ^{o}C. At this point, it can be concluded that the single phase perovskite membrane with highest bulk density can potentially be the dense perovskite membrane. Accordingly, LSGF 6428 sintering at 1250 ^{o}C, LSGF 6437 sintering at 1200 ^{o}C, LSGF 7328 sintering at 1250 ^{o}C, LSGF 7337 sintering at 1200 ^{o}C and LSGF 8228 sintering at 1200 ^{o}C are the potential dense perovskite membrane for oxygen separation.

Table 5.7 Physical property of perovskite membrane after sintering

Type	Sintering temperature (°C)	Weight (g)	Volume (*10⁻³cm³)	Bulk density (g/cm³)	Observed secondary phase
6428	1200	0.347	82.557	4.568	No
	1250	0.312	72.253	4.698	No
	1300	0.409	96.517	4.605	Traces
	1350	0.444	107.209	4.502	Traces
6437	1200	0.352	75.728	5.052	No
	1250	0.327	79.258	4.480	Traces
	1300	0.353	86.685	4.468	Traces
	1350	0.355	86.875	4.436	Traces
7328	1200	0.385	84.758	4.935	No
	1250	0.377	81.556	5.017	No
	1300	0.347	79.321	4.741	Traces
	1350	0.411	97.775	4.570	Traces
7337	1200	0.370	77.789	5.158	No
	1250	0.396	87.623	4.905	Traces
	1300	0.315	70.927	4.821	Yes
	1350	0.381	87.612	4.718	Yes
8228	1200	0.332	72.773	4.960	No
	1250	0.355	80.546	4.783	Traces
	1300	0.420	97.988	4.660	Traces
	1350	0.336	84.121	4.342	Traces

CHAPTER 6

CONCLUSION AND SUGGESTION

6.1 Conclusion

6.1.1 Perovskite compound

Fine particle strontium and iron substituted lanthanum gallates $La_{1-x}Sr_xGa_{1-y}Fe_yO_{3-\delta}$, where Sr = 0.5 and Fe = 0.8, Sr = 0.4 and Fe = 0.6-0.8, Sr = 0.3 and Fe = 0.3-0.8, and Sr = 0.2 and Fe = 0.3-0.8 had been synthesized by a modified citrate method.

La in A-site and Ga in B-site of ABO_3 based perovskite substituted with Sr and Fe showed the cubic structure. The single phase compound or the single phase with traces of secondary phase was obtained when La is 0.6 and Ga<3, La is 0.7 and Ga<0.4, and La is 0.8 and Ga<0.4.

By XRD, it can be concluded that LSGF 6428, LSGF 7328, LSGF 8228 and LSGF 8237 are the single phase while LSGF 6437, LSGF 7337, LSGF 7346, and LSGF 8246 are also single phase regardless of the traces of secondary phase. However, LSGF 5528, LSGF 7355, LSGF 7364, LSGF 8255 and LSGF 8264 were not single phase due to the existence of the secondary phase. It indicated that the secondary phase increased when the amount of Sr or Ga increased because of the incomplete substitution of La and Ga sites by Sr and Fe, respectively.

6.1.2 Perovskite membrane

Apparently, Sr and Fe content affected the morphology of perovskite membranes. With higher Sr content, the melting point of the membrane decreases. Thus higher Sr content could induce the welding of perovskite membrane. As a result, at the same sintering temperature, the grain size and density of LSGF 6428 were larger than of LSGF 7328 and LSGF 8228, respectively.

With higher Fe content, more $LaFeO_3$ structure, this is more stable than $LaGaO_3$. Therefore at the same sintering temperature, the welding of LSGF 7337 and LSGF 8246 can occur more readily than LSGF 7328 and LSGF 8228, respectively. In addition, the grain size and density of perovskite increased with the increase in sintering temperature due to the welding of perovskite.

The bulk density of membrane was higher with the increase in sintering temperature. When the phase of membrane was transformed to the secondary phase, the bulk density decreased. This observation can be explained in term of Ga vaporization at high temperature.

Accordingly, it can be concluded that the density of perovskite membrane depended on Sr content, Ga content and sintering temperature but the density is decreased when the secondary phase is formed. The highest dense single phase perovskite membranes for each composition are listed in Table 6.1.

Table 6.1 The highest dense single phase perovskite membranes for each composition

Composition	Sintering temperature (^{o}C)	Bulk density (g/cm^3)	Single phase
LSGF 6428	1250	4.698	Yes
LSGF 6437	1200	5.052	Yes
LSGF 7328	1250	5.017	Yes
LSGF 7337	1200	5.158	Yes
LSGF 8228	1200	4.960	Yes

6.2 Suggestion

1. The higher dense membrane shall be prepared by using isopressing machine instead of uniaxial pressing machine.

2. The testing on oxygen permeation to prove the dense perovskite membrane for oxygen separation membrane in partial oxidation process shall be investigated.

3. The modification of the perovskite membrane surface, for improving oxygen permeation by coating with either the same or the other type of perovskite shall be explored.

REFERENCES

1. Henrici, G.; and Olive, S. "The fischer-tropsch synthesis: molecular weight distribution of primary products and reaction mechanism" *Angew. Chem. Int. Ed.* 15(3) **(1976)**: 136-141.

2. Tsai, C. Y.; Dixon, A. G.; Moser, W. R.; and Ma, Y. H. "Dense perovskite membrane reactors for partial oxidation of methane to syngas" *Ceramics Processing* 43 **(1997)**: 2741-2750.

3. Gaudernack, B.; and Lynum, S. "Hydrogen from natural gas without release of CO_2 to the atmosphere" *Int. J. Hydrogen Energy* 23(12) **(1998)**: 1087-1093.

4. Paturzo, L.; and Basile, A. "Methane conversion to syngas in a composite palladium membrane reactor with increasing number of Pd layers" *Ind. Eng. Chem. Res.* 41 **(2002)**: 1703-1710.

5. Argonne, I. L. "Material scientists at argonne national laboratory" *Chemical Engineering Progress* **(1995):** 11-14.

6. Tantayanon, S.; Yeyongchaiwat, J.; Lou, J.; and Ma, Y. "Synthesis and characterization of Sr and Fe substituted $LaGaO_3$ perovskites and membranes." *Separation and Purification Technology* 32 **(2003)**: 319-326.

7. Pena, M. A.; and Fierro, J. L. G. "Chemical structures and performance of perovskite oxides" *Chem. Rev.* 101 **(2001)**: 1981-2017.

8. Rao, C. N. R.; Gopalakrishnan, J.; and Vidyasagar, K. "Superstructure, ordered defects and nonstoichiometry in metal oxides of perovskite and related structure" *Indian J. Chem.* 23A(4) **(1984)**: 265-284.

9. Gschneider, K. A. Jr.; and Eyring, L., Eds. Handbook of the physics and chemistry of rare earths, North-Holland Publishers, Amsterdam, 1979: 553.

10. Teraoka, Y.; Nobunaga, T.; and Yamazoe, N. "Effect of cation substitution on the oxygen semipermeability of perovskite-type oxide" *Chem. Lett.* **(1988)**: 503-506.

11. Tejuca, L. G.; and Fierro, J. L. G. "Properties and applications of perovskite-type oxides" Marcel Dekker, Inc., New York 1993: 3-14.

12. Reed, J. S. "Flocculants, binders, and bonds" in introduction of the principles of ceramic processing, John-Wiley & Sons, New York, 1985.

13. Johnson, D. W. "Reactive powders from solution" in ceramic processing before firing, onoda, G. Y.; Hench, Jr., L. L. (Eds.), Wiley, New York, 1978, 125-139.

14. Schnettler, F. J.; Monforte, F. R.; and Rhodes, W. H. "A cryochemical method for preparing ceramic materials" in science of ceramics, Stewart, G. H. (Ed.), The British Ceramic Society, Stoke-on Trent, U. K., 1968: 79-90.

15. Johnson, D. W. "Sol-gel processing ceramics and glass" *Am. Ceram. Soc. Bull.* 64(12) (**1985**): 1597-1602.

16. Pechini, M. "Method of preparing lead and alkaline-earth titanates and niobates and coating method using the same to form a capacitor" U. S. Patent No. 3,330,679, July 11, 976.

17. Baythoun, M. S. G.; and Sale, F. R. "Production of strontium-substituted lanthanum manganite perovskite powder by the amorphous citrate process" *J. Mater. Sci.* 17 (**1982**): 2757-2769.

18. Blank, D. H. A.; Kruidhof, H.; and Flokstra, J. "Preparation of $YBa_2Cu_3O_{7-\delta}$ by citrate synthesis and pyrolysis" *J. Phys. D: Appl. Phys.* 21 (**1988**): 226-227.

19. Chick, L. A. "Synthesis of oxide ceramic powders by the glycine-nitrate process" *Mat. Lett.* 10 (**1990**): 1-2.

20. Teraoka, Y.; Kakebayashi, H.; Taura, Y.; Moriguchi, I.; and Kagawa, S. "Malic acid-aided synthesis of perovskite type oxides of the La-Co and La-Mn systems and their catalytic property" *Kidorui* 30 (**1997**): 124-125.

21. Suresh, K.; Panchapagesan, T. S.; and Patil, K. C. "Synthesis and properties of $La_{1-x}A_xFeO_3$" *Solid State Ionics* 126 (**1999**): 299-305.

22. Richerson, D. W. "Modern ceramic engineering, properties, processing, and use in design," 2nd ed., 1992: 378-381.

23. Kuczynski, G. C. "Transactions of the american institute of mining, metallurgical, and petroleum engineering" *J. Appl. Phys.* 21 (**1950**): 632.

24. Burke, J. E.; and Rosolowski, J. H. "Sintering" in treatise on solid state chemistry, vol. 4; Reactivity of Solids, Hannay, N. B. (Ed.), Plenum Press, New York, 1921.

25. Sammells, A. F.; Schwartz, M.; Mackay, R. A.; Barton, T. F.; and Peterson, D. R. "Catalytic membrane reactors for spontaneous synthesis gas production" *Catalysis Today* 56 (**2000**): 325–328.

26. Sherman, J. Xu.; and Thomson, W. J. "Oxygen permeation rates through ion-conducting perovskite membranes" *Chemical Engineering Science* 54 (**1999**): 3839-3850.

27. Hassel, V. B. A.; Kawada, T.; Sakai, N.; Yokokawa, H.; Dokiya, M.; and Bouwmeester, H.J.M. "Oxygen permeation modeling of perovskites" *Solid State Ionics* 66 (**1993**): 295-305.

28. Li, S.; Qi, H.; Xu, N.; and Shi, J. "Tubular dense perovskite type membranes preparation, sealing, and oxygen permeation properties" *Ind. Eng. Chem. Res.* 38 (**1999**): 5028-5033.

29. Li, S.; Jin, W.; Huang, P.; Xu, N.; Shi, J.; Michael, Z. C. H.; Payzant, E. A.; and Ma, Y. H. "Perovskite-related ZrO_2-Doped $SrCo_{0.4}Fe_{0.6}O_{3-\delta}$ membrane for oxygen permeation" *AIChE J.* 45 (**1999**): 276-284.

30. De Bruin, H. J.; Moodie, A. F.; and Warble, C. E. "Ceramic-metal reaction welding" *J. Mat. Sci.* 7 (**1972**): 909-918.

31. Bailey, F. P.; and Black, K. J. T. "Gold-to-alumina solid state reaction bonding" *J. Mat. Sci.* 13 (**1978**): 1045-1052.

32. Ishihara, T.; Tsuruta, Y.; Todaka, T.; Nishiguchi, and H.; Takita, Y. "Fe doped $LaGaO_3$ perovskite oxide as an oxygen separatingmembrane for CH_4 partial oxidation" *Solid State Ionics* 152 (**2002**): 709– 714.

33. Chen, C.H.; Bouwmesster, H.J.M.; van Doorn, R.H.E.; Kruidhof, H.; and Burggraaf, A.J. "Oxygen permeation of $La_{0.3}Sr_{0.7}CoO_{3-\delta}$" *Solid State Ionics* 98 (**1997**): 7–13.

34. Patrakeev, M. V.; Mitberg, E. B.; Lakhtin, A. A.; Leonidov, I. A.; Kozhevnikov, V. L.; Kharton, V. V.; Avdeev, M.; and Marques, F. M. B. "Oxygen nonstoichiometry, conductivity, and seebeck coeffcient of $La_{0.3}Sr_{0.7}Fe_{1-x}Ga_xO_{2.65+\delta}$ perovskites" *Solid State Chemistry* 167 (**2002**): 203-213.

35. Tu, H.Y.; Takeda, Y.; Imanishi, N.; and Yamamoto, O. "$Ln_{0.4}Sr_{0.6}Co_{0.8}Fe_{0.2}O_{3-\delta}$ (Ln La, Pr, Nd, Sm, Gd) for the electrode in solid oxide fuel cells" *Solid State Ionics* 117 (**1999**): 277–281.

36. Ishihara, T.; Yamada, T.; Akbay, Y.; and Takita, Y. "Partial oxidation of methane over fuel cell type reactor for simultaneous generation of synthesis gas and electric power" *Chemical Engineering Science* 54 (**1999**): 1535-1540.

37. Balachandran, U.; Dusek, J.T.; Mieville, R.L.; Poeppel, R.B.; Kleefisch, M.S.; Pei, S.; Kobylinski, T.P.; Udovich, C.A.; and Bose, A.C. "Dense ceramic membranes for partial oxidation of methane to syngas" *Appl. Catal. A: Gen.* 133 (**1995**): 19–29.

38. Wang, H.; Cong, Y.; and Yang, W. "Partial oxidation of ethane to syngas in an oxygen-permeable membrane reactor" *Journal of Membrane Science* 209 (**2002**): 143–152.

39. Zeng, Y.; and Lin Y.S. "A transient TGA study on oxygen permeation properties of perovskite-type ceramic membrane" *Solid State Ionics* 110 (**1998**): 209–221.

40. Tan, L.; Gu, X.; Yang, L.; Jin, W.; Zhang, L.; and Xu, N. "Influence of powder synthesis methods on microstructure and oxygen permeation performance of $Ba_{0.5}Sr_{0.5}Co_{0.8}Fe_{0.2}O_{3-\delta}$ perovskite-type membranes" *Journal of Membrane Science* 212 (**2003**): 157–165.

41. Stevenson, J. W.; Armstrong, T. R.; Pederson, L. R.; Li, J.; Lewinsohn, C. A.; and Baskaran, S. "Effect of A-site cation nonstoichiometry on the properties of doped lanthanum gallate" *Solid State Ionics* 113 (**1998**): 571-583.

42. Ishihara, T.; Matsuda, H.; and Takita, Y. "Doped LaGaO$_3$ perocskite type oxide as a new oxide conductor" *J. Am. Chem. Soc*. 116 (**1994**): 3801-3803.

43. Labye, D.; Poulsen, F. W.; and Mogensen, M. "Conductivity of A- and B- site doped LaAlO$_3$, LaGaO$_3$, LaScO$_3$ and LaInO$_3$ perovskites" *Solid State Ionics* 128 (**2000**): 91-103.

44. Teraoka, Y.; Zhang, H. M.; Furukawa, S.; and Yamazoe, N. "Oxygen permeation through perovskite-type oxides" *Chem. Lett*. (**1985**): 1743-1746.

45. Li, S.; Jin, W.; Huang, P.; Xu, N.; Shi, J.; Lin, Y. S.; Hu, M. C.; and Payzant, E. A. "Comparison of oxygen permeability and stability of perovskite La$_{0.2}$A$_{0.8}$Co$_{0.2}$Fe$_{0.8}$O$_{3-\delta}$ (A = Sr, Ba and Ca) membranes" *Ind. Eng. Chem. Res*. 38 (**1999**): 2963-2972.

46. Gharbage, B.; Figueiredo, F. M.; Beaker, R. T.; and Marques, F. M. B. "Electrochemical permeability of La$_{0.9}$Sr$_{0.1}$Ga$_{1-x}$Fe$_x$O$_{3-\delta}$" *Electrochimica Acta* 45 (**2000**): 2095-2099

47. Ishihara, T.; Yamada, T.; Arikawa, H.; Nishiguchi, H.; and Takita, Y. "Mixed electronic-oxide Ionic conductivity and oxygen permeating property of Fe-, Co- or Ni-doped LaGaO$_3$ perovskite oxide" *Solid State Ionics* 135 (**2000**): 631-636.

48. Ming, Q.; Nersesyan, M. D.; Wagner, A.; Ritchie, J.; Richardson, J. T.; Luss, D.; Jacobson, A. J.; and Yang, Y. L. "Combustion synthesis and characterization of Sr and Ga doped LaFeO$_3$" *Solid State Ionics* 122 (**1999**): 113-121.

49. Bouwmeester, H. J. M.; Burggraaf, A. J.; and Gellings, D. J. (Eds.) The CRC Handbook of solid state electrochemistry, CRC Press, 1997.

50. Barnard, J.A.; and Bradley, J.N. Flame and Combustion 2nd ed., Chapman and Hall, N.Y., USA, 1991.

51. Kwon, Y. T.; Lee, I. M.; Lee, W.I.; Kim, C.J.; and Yoo, I.K. "Effect of sol–gel precursors on the grain structure of PZT thin films" *Mater. Res. Bull*. 34(5) (**1999**): 749-760.

52. Kleveland K.; Einarsrud M. A.; and Grande, T. "Sintering of LaCoO$_3$-based Ceramics*" J. Eur. Ceram. Soc*. 20 (**2000**): 185-193.

53. Mori, M.; Hiei, Y.; and Sammes, N. M. "Sintering behavior and mechanism of Sr-doped lanthanum chromites with A site excess composition in air" *Solid State Ionics* 123 **(1999)**: 103-111.

54. Mori, M.; Hiei, Y.; and Sammes, N. M. "Sintering behavior of Ca- or Sr-doped $LaCrO_3$ perovskites including second phase of $AECrO_4$ (AE = Sr, Ca) in Air" *Solid State Ionics* 135 **(2000)**: 743-748.

55. Khanlou, A.; Tietz, F.; and Stover, D. "Material properties of $La_{0.8}Sr_{0.2}Ga_{0.9+x}Mg_{0.1}O_{3-\delta}$ as a function of Ga content" *Solid State Ionics* 135 **(2000)**: 543-547.

56. Yeyongchaiwat, J. "Synthesis and characterization of $La_{1-x}Sr_xGa_{1-y}Fe_yO_{3-\delta}$ perovskite membrane." Doctoral dissertation, Department of Chemical Technology, Faculty of Science, Chulalongkorn University.

57. Cullity, B. D. Elements of X-ray Diffraction 2nd ed., Addison-Wesley Publishing Company, Inc., MA, USA, 1978.

58. Hayashi, H.; Suzuki, M.; and Inaba, H. "Thermal expansion of Sr- and Mg-doped $LaGaO_3$" *Solid State Ionics* 128 **(2000)**: 131-139.

59. Yamaji, K.; Negishi, H.; Horita, T.;Sakai, N.; and Yokokawa, H. "Vaporization process of Ga form doped LaGaO3 electrolytes in reducing atmospheres" *Solid State Ionics* 135 **(2000)**: 389-396.

60. Yamaji, K.; Ishikawa, M.; Horita, T.; Sakai, N.; and Yokokawa, H. "Chemical stability of the $La_{0.9}Sr_{0.1}Ga_{0.8}Mg_{0.2}O_{2.85}$ electrolyte in a reducing atmosphere" *Solid State Ionics* 121 **(1999)**: 217-224.

APPENDICES

APPENDIX A

Tolerance number [58]

Goldschmidt (1926) defined the tolerance limits of the size of ions through a tolerance factor, t as Equation (A.1)

$$t = (r_A + r_O)/ [\sqrt{2}\ (r_B + r_O)] \qquad (A.1)$$

Where r_A, r_B, and r_O are the radii of respective ions. For the substituted perovskite at A and B site, $A_{1-x}A'_xB_{1-y}B'_yO_{3-\delta}$, r_A and r_B were calcuated from the sum of each metal at A site and B site, respectively, time its compostition. The atomic weight, ionic charge, coordination number, and ionic radius of all concerned metals were shown in Table A.1

Table A.1 Atomic weight, ionic charge, coordination number, and ionic radius of concerned metals

Metal	Atomic weight	Ionic charge	Coordination No.	Ionic radius (Å)
La	138.92	3+	12	1.36
Fe	55.85	3+	6	0.55
Ga	69.72	3+	6	0.62
Ba	137.36	2+	12	1.61
Sr	87.62	2+	12	1.44
Co	58.94	2+	6	0.65
O	16.00	2-	6	1.40

Therefore, as Equation A.1 the tolerance number of perovskite compounds such as LSGF 6428 was calculated as below.

$$\text{Tolerance number of LSGF6428} = \frac{1.36*0.6+1.44*0.4+1.40}{\sqrt{2}\ (0.55*0.8+0.62*0.2+1.40)}$$

$$= 1.01$$

Bulk density

Bulk density (D) can be calculated from mass and volume as shown in Equation (A.2)
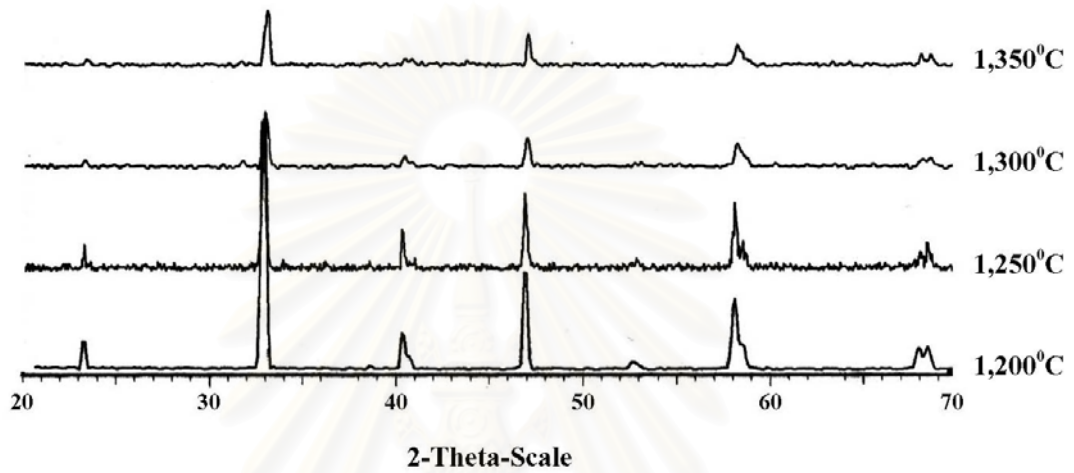
$$D = Mass/ \pi R^2 *h \qquad (A.2)$$
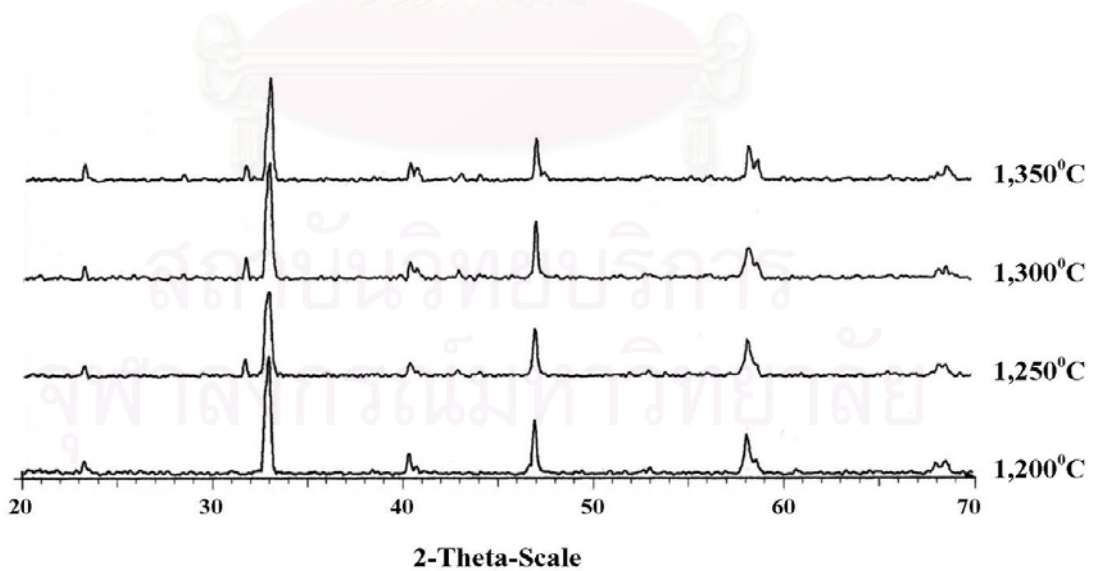
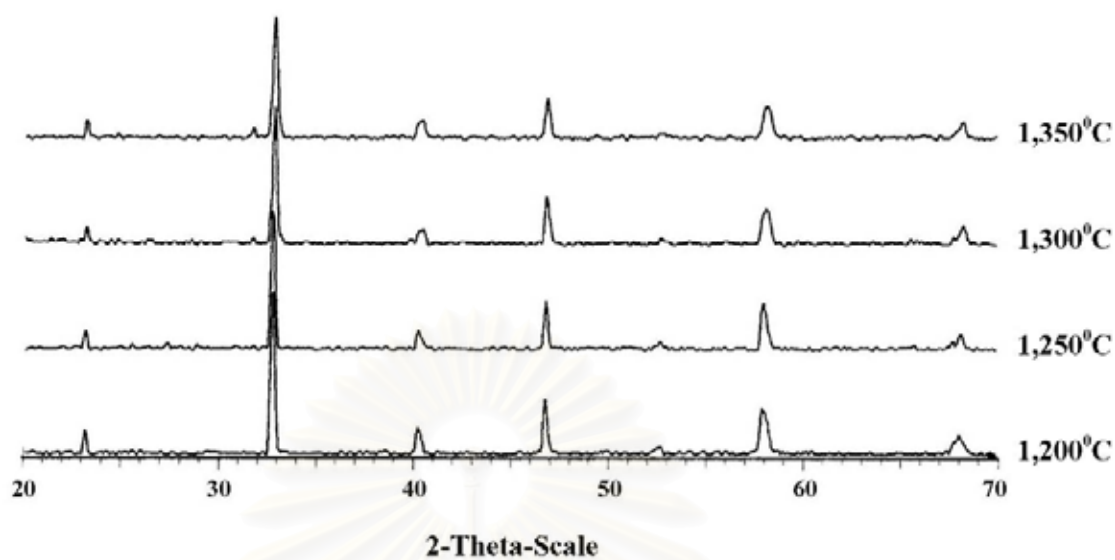Where R is the radius and h is the thickness of membrane

APPENDIX B

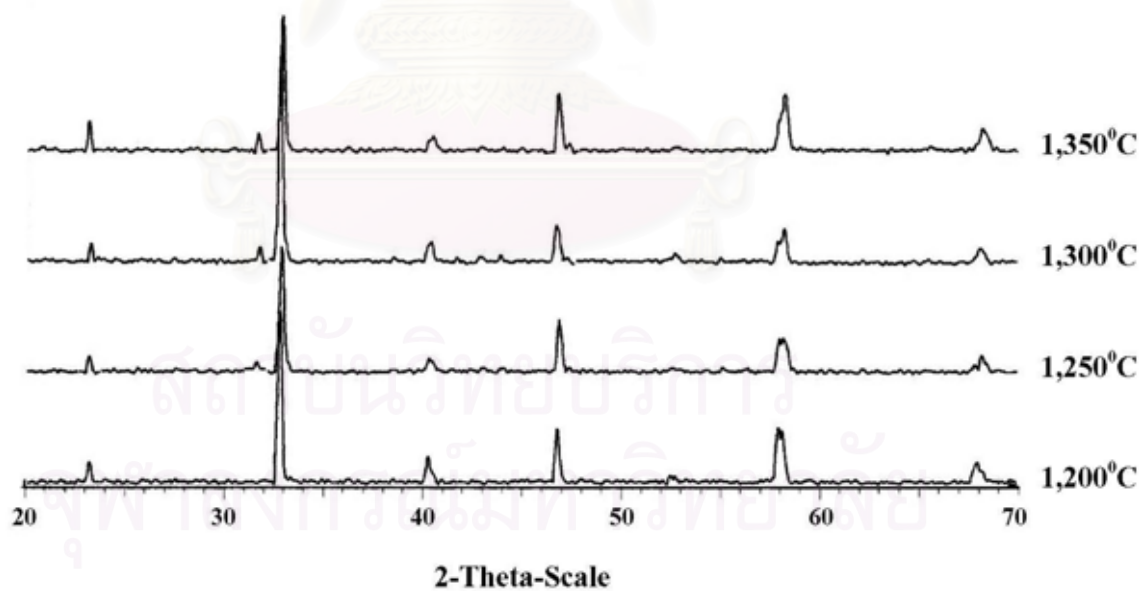**XRD patterns of membranes after sintering at various temperatures**

Figure B-1 XRD patterns of LSGF 6428 perovskite membrane after sintered at 1,200-1,350^{o}C

Figure B-2 XRD patterns of LSGF 6437 perovskite membrane after sintered at 1,200-1,350^{o}C
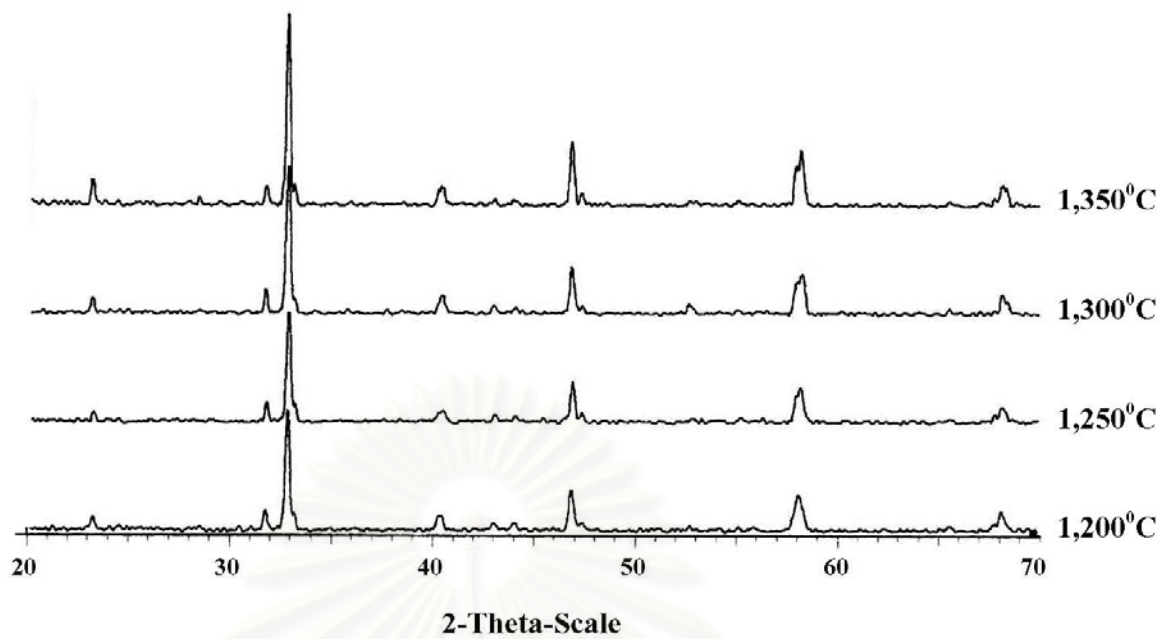
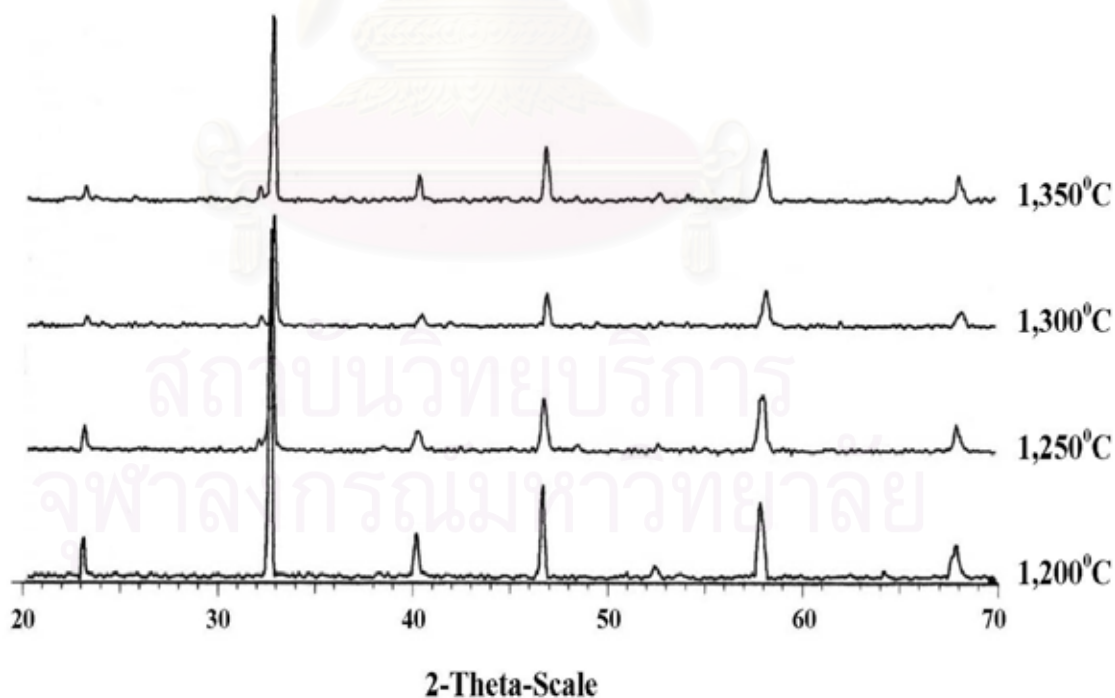**Figure B-3** XRD patterns of LSGF 7328 perovskite membrane after sintered at
1,200-1,350°C

Figure B-4 XRD patterns of LSGF 7337 perovskite membrane after sintered at
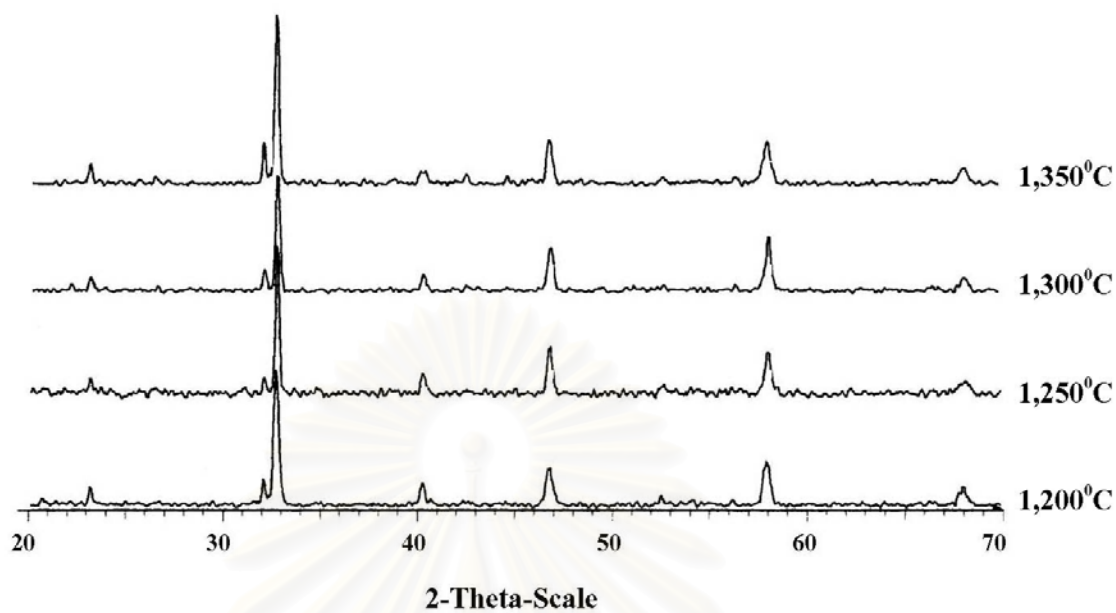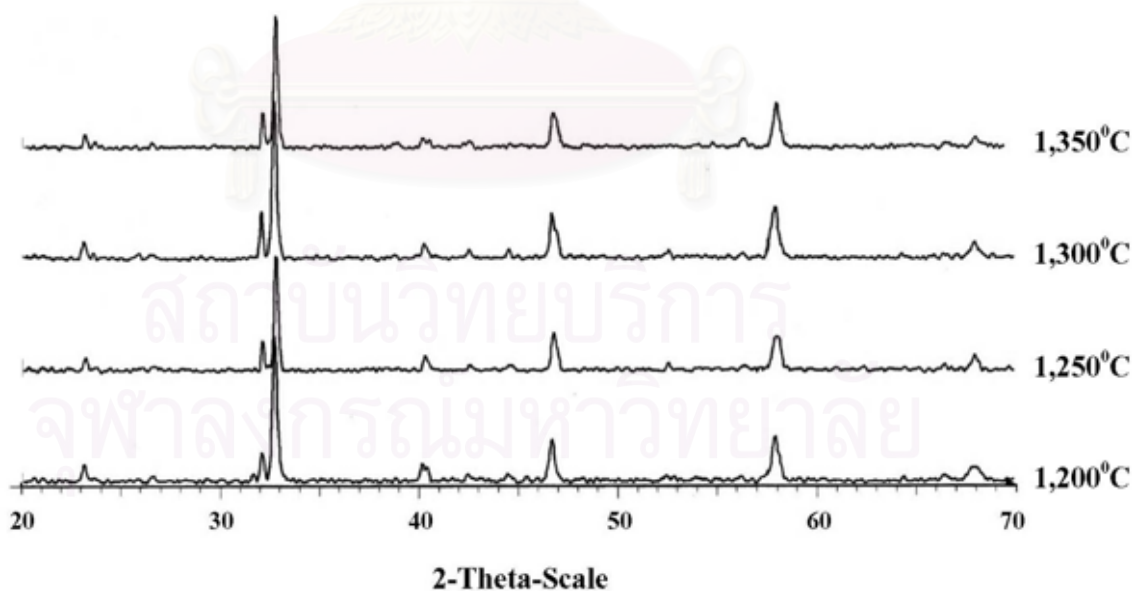1,200-1,350°C

Figure B-5 XRD patterns of LSGF 7346 perovskite membrane after sintered at
1,200-1,350^{o}C

Figure B-6 XRD patterns of LSGF 8228 perovskite membrane after sintered at
1,200-1,350^{o}C

Figure B-7 XRD patterns of LSGF 8237 perovskite membrane after sintered at
1,200-1,350°C

Figure B-8 XRD patterns of LSGF 8246 perovskite membrane after sintered at
1,200-1,350°C

VITA

Mr. Sarawut Tanyong was born on November 1, 1978, in Chonburi, Thailand. He received his B.Sc. in Industrial Chemistry from King Mongkut's Institute of Technology Ladkrabang in 2001. He attended the Master′s Degree Program of Petrochemistry and Polymer Science, Faculty of Science, Chulalongkorn University and finished his study in 2003.